

UNILocPro: Unified Localization Integrating Model-Based Geometry and Channel Charting

Yuhao Zhang, Guangjin Pan, *Member, IEEE*, Musa Furkan Keskin, *Member, IEEE*,
Ossi Kaltiokallio, *Member, IEEE*, Mikko Valkama, *Fellow, IEEE*, and Henk Wymeersch, *Fellow, IEEE*

Abstract—In this paper, we propose a unified localization framework (called UNILocPro) that integrates model-based localization and channel charting (CC) for mixed line-of-sight (LoS)/non-line-of-sight (NLoS) scenarios. Specifically, based on LoS/NLoS identification, an adaptive activation between the model-based and CC-based methods is conducted. Aiming for unsupervised learning, information obtained from the model-based method is utilized to train the CC model, where a pairwise distance loss (involving a new dissimilarity metric design), a triplet loss (if timestamps are available), a LoS-based loss, and an optimal transport (OT)-based loss are jointly employed such that the global geometry can be well preserved. To reduce the training complexity of UNILocPro, we propose a low-complexity implementation (called UNILoc), where the CC model is trained with self-generated labels produced by a single pre-training OT transformation, which avoids iterative Sinkhorn updates involved in the OT-based loss computation. Extensive numerical experiments demonstrate that the proposed unified frameworks achieve significantly improved positioning accuracy compared to both model-based and CC-based methods. Notably, UNILocPro with timestamps attains performance on par with fully-supervised fingerprinting despite operating without labelled training data. It is also shown that the low-complexity UNILoc can substantially reduce training complexity with only marginal performance degradation.

Index Terms—localization, model-based localization, channel charting, machine learning, unsupervised learning, optimal transport.

I. INTRODUCTION

Wireless communication systems (e.g., 5G and 6G) provide opportunities for high-precision localization, even in global navigation satellite system (GNSS)-challenged environments [2]–[4]. In general, wireless localization methods fall into two main categories: (1) model-based methods relying on channel parameter estimation and geometric relationships [5]–[8], and (2) data-driven methods leveraging machine learning (ML) to infer user position from channel state information (CSI) [9]–[12]. Model-based methods typically exploit the line-of-sight (LoS) path (provides the most direct and reliable information about the user location), whose parameters (e.g., time-of-arrival (ToA), angle-of-arrival (AoA), time-difference-of-arrival

This work has been supported, in part, by the European Union through the project ISLANDS - Grant agreement n. 101120544, by the Swedish Research Council (VR) through the project 6G-PERCEF under Grant 2024-04390, and by Business Finland under the 6G-ISAC project. (*Corresponding author: Guangjin Pan.*)

Yuhao Zhang, Guangjin Pan, Musa Furkan Keskin, and Henk Wymeersch are with the Department of Electrical Engineering, Chalmers University of Technology, 41296 Gothenburg, Sweden (e-mail: {yuhaozh, guangjin.pan, furkan, henkw}@chalmers.se).

Ossi Kaltiokallio and Mikko Valkama are with the Unit of Electrical Engineering, Tampere University, 33100 Tampere, Finland (e-mail: {ossi.kaltiokallio, mikko.valkama}@tuni.fi).

Part of this work has been presented in our previous conference paper [1], which is a special case of the proposed localization framework.

(TDoA)) are estimated using algorithms such as multiple signal classification (MUSIC) or orthogonal matching pursuit (OMP) [13], and then mapped to the user location via geometric relationships. These methods perform well in LoS scenarios (e.g., user 1 in Fig. 1) but degrade under non-line-of-sight (NLoS) conditions due to LoS blockage (e.g., user 2 in Fig. 1).¹ Although advanced techniques can exploit NLoS paths, they are often complex and scenario-specific (e.g., relying on specular reflections) [5], [6], [8]. On the contrary, data-driven methods hold some promise for NLoS scenarios, but suffer from certain drawbacks. For example, supervised learning, e.g., fingerprinting [9]–[11], requires extensive data measurement and collection for each specific setting, which may not be practical especially for dynamic environments, where fingerprints can become outdated with time and thus frequent data re-measurement and retraining are required. As an unsupervised learning technique that aims to generate a mapping from high-dimensional CSI to a low-dimensional space (called channel chart), channel charting (CC) can learn the relative geometry based on CSI without the need for labeled data, while it would usually yield position estimates that are highly distorted [14], [15]. In order to preserve the global geometry, side information and/or model-based methods can be utilized in CC for absolute localization [16]–[18].

Particularly interesting is the use of CC for absolute localization, which requires auxiliary information, e.g., anchor locations or map information. With a set of labeled CSIs, a localization penalty similar to fingerprinting can be incorporated into the loss function to optimize the CC model [15], [19], [20]. In [17], [21]–[24], anchor points with known positions are used to find an affine transformation matching the channel chart with the global coordinates. All the above methods are semi-supervised, requiring pre-measured anchor locations or labeled data, which share the drawbacks of fingerprinting. To mitigate these issues, map-assisted approaches can exploit, for example, building floor plans or street maps to align the channel chart with the global coordinates. In [25], a CC method is proposed for indoor localization, where a Siamese neural network (NN) is trained to coherently optimize a pairwise distance loss and a Sinkhorn distance between the channel chart and the topological map. In [26], a velocity-assisted CC is proposed for indoor scenarios where the distance between two CSI samples is calculated based on velocity information (measured by deploying pedestrian dead reckoning or odometry systems) and an affine transformation is learned to match the generated channel chart and building floor plans.

¹In this paper, NLoS scenarios refer to scenarios where the LoS path is blocked. Conversely, LoS scenarios describe cases where the LoS path exists, regardless of whether NLoS paths are present or not.

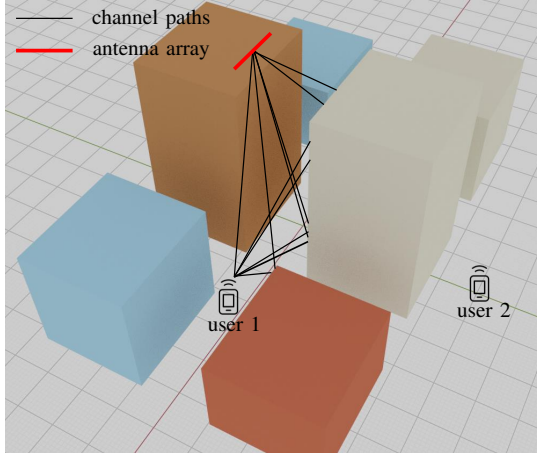


Fig. 1: A street canyon scenario [27], where channel paths are shown for user 1 for example. Note that user 1 is a LoS user, while user 2 is a NLoS user as its LoS path is blocked by a building.

To improve robustness, interpretability, and accuracy of localization, model-based and data-driven methods can be integrated to exploit their complementary strengths. In the literature, model-based localization has also been used to assist CC in achieving unsupervised absolute localization. For example, a CC technique is proposed in [18] for an indoor scenario by incorporating ToA measurements and laser scanner data into the loss function. In [16], an augmented CC approach is proposed for an indoor scenario, where the joint TDoA and AoA likelihood is included in the NN training loss. In [28], a self-supervised CC-based localization is proposed for distributed systems by leveraging TDoA measurements and multiple transmission reception point (TRP) locations. However, in [18], an additional laser scanner system is required to calculate the distance between two CSI samples, which induces extra cost and complexity; [28] classifies the NLoS paths as foes and consequently filters out the NLoS information, making it unavailable for localization; the cosine-based dissimilarity used in [16] performs inadequately in NLoS scenarios, as will be shown in Sec. VII. In summary, in-depth integration of model-based localization and CC remains an open challenge and has not been addressed to date.

Moreover, for CC-based localization, it is crucial to select or design an appropriate dissimilarity metric that can adequately achieve accurate global positioning. Since the dissimilarity metric computed solely from CSIs is highly related to channel characteristics [14], [17], [21], [22], its positioning performance is sensitive to channel conditions, e.g., LoS/NLoS conditions. In the literature, CC-based localization is studied mainly for LoS dominant environments [17], [22], [24], [26], and the above model-assisted works [16], [18], [28] require LoS conditions for absolute positioning.² Therefore, it remains unclear how to perform CC-based localization in mixed LoS/NLoS scenarios. For example, whether existing dissimilarity metrics can adequately preserve local and global geometry in mixed LoS/NLoS scenarios (especially in LoS and NLoS transition regions where an abrupt change of CSI occurs) or whether new metrics are needed for global localization.

²In this paper, we use ‘‘LoS dominant’’ to represent the scenario where most of the user positions in the system have a LoS path to the base station (BS).

In this paper, we aim to design unified localization frameworks that integrate model-based and fully-unsupervised CC-based methods in challenging mixed LoS/NLoS scenarios by exploiting available map information (only a coarse map is required, e.g., a street or floor plan, which is usually available for many cities and buildings). Extending our prior research [1], we integrate CC-based localization to build a more comprehensive unified framework, further enhancing positioning performance. Furthermore, we conduct systematic numerical experiments to provide a thorough comparative evaluation and analysis. The main contributions of this work are as follows:

- **Unified model- and CC-based localization framework for mixed LoS/NLoS scenarios (Sec. IV):** We propose a unified localization framework (UNILocPro) that integrates model-based and CC-based methods for mixed LoS/NLoS environments. Based on LoS/NLoS identification, we apply the model-based method to the identified LoS users and the CC-based method to the identified NLoS users. To enable unsupervised learning, channel parameters estimated from CSI are used to train the CC model, preserving the global spatial geometry. UNILocPro is unified in: (1) separate handling of LoS/NLoS users; (2) unsupervised learning driven by both model and data; and (3) a multi-component CC loss that exploits model and map information.
- **Novel dissimilarity metrics and multi-component loss design (Sec. V):** Using channel parameters extracted from the model-based method, we design effective dissimilarity metrics, including the generalized optimal sub-pattern assignment (GOSPA)-based, the Wasserstein-based, and their fusion, to preserve local geometry in CC. The global geometry is maintained by using model-based position estimates of identified LoS users as anchors and incorporating an optimal transport (OT)-based loss during training to align with the map. Additionally, when timestamps are available, a timestamp-based triplet loss can also be applied to further enhance the CC model.
- **Low-complexity implementation with pre-trained OT transformation (Sec. VI):** To reduce the high computational cost of the OT-based loss in the CC model, we propose a low-complexity approach (UNILoc) that replaces iterative OT execution during training with a single pre-trained OT transformation. Specifically, the CC model is trained using self-generated labels obtained from model-based position estimates and map information through OT alignment. This strategy greatly decreases training overhead and complexity while maintaining high positioning accuracy. In our experiments, UNILoc achieves a training complexity reduction of about $\mathcal{O}(N_u^2)$, where N_u is the number of data samples, and runs 4-5 times faster than UNILocPro.

Notations: We denote column vectors as bold-faced lower-case letters, \mathbf{a} , and matrices as bold-faced upper-case letters, \mathbf{A} . A column vector with a size of N whose entries are all equal to 1 is denoted as $\mathbf{1}_N$. The identity matrix of size $N \times N$ is denoted as \mathbf{I}_N . The transpose and conjugate transpose operations are

denoted by $(\cdot)^\top$ and $(\cdot)^\mathsf{H}$, respectively. The i -th element of a vector and the (i, j) -th element of a matrix are denoted by $[\mathbf{a}]_i$ and $[\mathbf{A}]_{i,j}$, respectively. \otimes represents the Kronecker product and \oslash represents the element-wise division. $\text{vec}(\cdot)$ denotes the matrix vectorization operator and $\text{diag}(\cdot)$ denotes the diagonalization operator. $\|\cdot\|_2$ and $\|\cdot\|_F$ are the Euclidean norm and the Frobenius norm, respectively. $\langle \cdot, \cdot \rangle_F$ represents the Frobenius dot product.

II. SYSTEM MODEL

We consider a single-cell orthogonal frequency division multiplexing (OFDM) system, where a BS equipped with M antennas serves multiple single-antenna users over N_c subcarriers (with Δ_f being the subcarrier spacing). A dedicated sequence of pilots is transmitted by each user such that its associated CSI can be estimated by the BS. We assume perfect channel estimation at the BS, and the CSI from user i at all subcarriers is denoted by $\mathbf{H}_i \in \mathbb{C}^{M \times N_c}$. Our goal is to estimate the position of each user, denoted by $\mathbf{p}_i = [x_i, y_i, z_i]^\top$, based solely on its associated CSI, i.e., $\hat{\mathbf{p}}_i = f_e(\mathbf{H}_i)$, $\forall i$, where $\hat{\mathbf{p}}_i$ is the estimate of \mathbf{p}_i and $f_e(\cdot)$ is a position estimation function.

A. Channel Model

Considering the multi-path effect, the frequency domain channel matrix for user i can be modeled as $\mathbf{H}_i = \sum_{l=1}^{L_i} \beta_l^i \mathbf{a}_t(\theta_l^i) \mathbf{b}^\top(\tau_l^i)$, $\forall i$, where there are L_i channel paths for user i [29]–[31]; β_l^i , θ_l^i , and τ_l^i are the complex channel gain, AoA, and ToA of the l -th path, respectively; $\mathbf{b}(\tau) \in \mathbb{C}^{N_c \times 1}$ is the frequency-domain steering vector, as given by $[\mathbf{b}(\tau)]_n = \exp[-j2\pi(n-1)\Delta_f\tau]$, $n = 1, 2, \dots, N_c$; $\mathbf{a}_t(\theta) \in \mathbb{C}^{M \times 1}$ is the array steering vector, which depends on the antenna array geometry. For example, when a uniform linear array (ULA) with inter-antenna separation of d is adopted, the steering vector is $[\mathbf{a}_t(\theta)]_m = \exp[j2\pi(m-1)\frac{d}{\lambda} \sin(\theta)]$, $m = 1, 2, \dots, M$, where $\lambda = c/f_c$ with c being the speed of light and f_c being the carrier frequency. The steering vector $\mathbf{a}_t(\theta)$ for uniform planar array (UPA) is referred to [11], [32].

With OFDM transmission and multi-antenna BS, channel parameters, including channel gain, AoA, and ToA for different channel paths, can be estimated from the CSI \mathbf{H}_i by channel estimation algorithms, e.g., the OMP algorithm [13], [30]. Specifically, with OMP, \hat{L}_i channel paths can be recovered with channel parameters $\{\hat{\beta}_l^i, \hat{\theta}_l^i, \hat{\tau}_l^i\}_{l=1,2,\dots,\hat{L}_i} = f_{\text{ce}}(\mathbf{H}_i)$ based on the CSI \mathbf{H}_i for user i , where $f_{\text{ce}}(\cdot)$ is the channel parameter estimation function. For more details, the reader is referred to Algorithm 1 of [30].

B. Map Information

We assume that a map of the environment is accessible, from which the region for all possible user positions can be extracted as $\mathcal{R} \subseteq \mathbb{R}^{3 \times 1}$ such that we have $\mathbf{p}_i \in \mathcal{R}$, $\forall i$. Moreover, the map enables us to determine whether a given point in \mathcal{R} has a LoS connection to the BS or not, based on which \mathcal{R} can be divided into $\mathcal{R}_{\text{LoS}} \subseteq \mathbb{R}^{3 \times 1}$ (the region for LoS user) and $\mathcal{R}_{\text{NLoS}} \subseteq \mathbb{R}^{3 \times 1}$ (the region for NLoS users), respectively, where $\mathcal{R}_{\text{LoS}} \cap \mathcal{R}_{\text{NLoS}} = \emptyset$ and $\mathcal{R}_{\text{LoS}} \cup \mathcal{R}_{\text{NLoS}} = \mathcal{R}$. In this work, the map serves only to identify possible user locations and LoS/NLoS regions, which necessitate a coarse map, e.g., a street or floor plan.

Without loss of generality, it is assumed that the prior information of the user distribution in \mathcal{R} is available, which can be characterized as a probability density function (PDF), denoted by $f_D(\mathbf{p})$, $\mathbf{p} \in \mathcal{R}$. Then, based on $f_D(\cdot)$, the PDFs for user distribution in LoS and NLoS regions, denoted by $f_D^{\text{LoS}}(\cdot)$ and $f_D^{\text{NLoS}}(\cdot)$ respectively, can be written as

$$f_D^{\text{LoS}}(\mathbf{p}) = \frac{f_D(\mathbf{p})}{\int_{\mathbf{p}' \in \mathcal{R}_{\text{LoS}}} f_D(\mathbf{p}') d\mathbf{p}'}, \quad \mathbf{p} \in \mathcal{R}_{\text{LoS}}, \quad (1)$$

$$f_D^{\text{NLoS}}(\mathbf{p}) = \frac{f_D(\mathbf{p})}{\int_{\mathbf{p}' \in \mathcal{R}_{\text{NLoS}}} f_D(\mathbf{p}') d\mathbf{p}'}, \quad \mathbf{p} \in \mathcal{R}_{\text{NLoS}}, \quad (2)$$

where \mathbf{p}' represents a user position in \mathcal{R} . Note that if the real prior information of user distribution is not accessible, uniform distribution in \mathcal{R} can be adopted as a default assumption such that we can have $f_D(\mathbf{p}) = \frac{1}{\int_{\mathbf{p}' \in \mathcal{R}} d\mathbf{p}'}$, $\mathbf{p} \in \mathcal{R}$, $f_D^{\text{LoS}}(\mathbf{p}) = \frac{1}{\int_{\mathbf{p}' \in \mathcal{R}_{\text{LoS}}} d\mathbf{p}'}$, $\mathbf{p} \in \mathcal{R}_{\text{LoS}}$, and $f_D^{\text{NLoS}}(\mathbf{p}) = \frac{1}{\int_{\mathbf{p}' \in \mathcal{R}_{\text{NLoS}}} d\mathbf{p}'}$, $\mathbf{p} \in \mathcal{R}_{\text{NLoS}}$, which solely depend on the map information.

III. PRELIMINARIES: GOSPA AND OT

A. GOSPA Metric

The GOSPA is a metric for measuring the difference between two sets of points, widely used in multi-target tracking and localization [30], [33], [34]. Consider two finite sets of points $\mathcal{X}_s = \{\mathbf{x}_s^1, \mathbf{x}_s^2, \dots, \mathbf{x}_s^{|\mathcal{X}_s|}\}$ and $\mathcal{X}_t = \{\mathbf{x}_t^1, \mathbf{x}_t^2, \dots, \mathbf{x}_t^{|\mathcal{X}_t|}\}$, where $|\mathcal{X}_s|$ and $|\mathcal{X}_t|$ are the cardinalities of the sets. Let $d(\mathbf{x}_s, \mathbf{x}_t)$ denote a distance for any $\mathbf{x}_s, \mathbf{x}_t \in \mathbb{R}^{N \times 1}$, based on which its cut-off version is defined as $d^{(\zeta)}(\mathbf{x}_s, \mathbf{x}_t) = \min(d(\mathbf{x}_s, \mathbf{x}_t), \zeta)$, where $\zeta > 0$ is a cut-off value that limits the maximum distance between two points, mitigating the influence of outliers and preventing extreme values from distorting the metric. Then, for $|\mathcal{X}_s| \leq |\mathcal{X}_t|$, the GOSPA metric is defined as [35]

$$\mathcal{G}_p^{(\zeta, \varpi)}(\mathcal{X}_s, \mathcal{X}_t) = \left(\min_{\pi \in \Pi_{|\mathcal{X}_t|}} \sum_{i=1}^{|\mathcal{X}_s|} d^{(\zeta)}(\mathbf{x}_s^i, \mathbf{x}_t^{\pi(i)})^p + \frac{\zeta^p}{\varpi} (|\mathcal{X}_t| - |\mathcal{X}_s|) \right)^{\frac{1}{p}}, \quad (3)$$

where the exponent $1 \leq p < \infty$ controls the penalization for inaccurate estimations; the parameter $0 < \varpi \leq 2$, together with ζ , controls the penalization for cardinality mismatch; $\Pi_{|\mathcal{X}_t|}$ is the set of all permutations of $\{1, \dots, |\mathcal{X}_t|\}$, with elements $\pi \in \Pi_{|\mathcal{X}_t|}$ being a sequence of indices $(\pi(1), \dots, \pi(|\mathcal{X}_t|))$. Note that if $|\mathcal{X}_s| > |\mathcal{X}_t|$, the GOSPA metric is $\mathcal{G}_p^{(\zeta, \varpi)}(\mathcal{X}_s, \mathcal{X}_t) = \mathcal{G}_p^{(\zeta, \varpi)}(\mathcal{X}_t, \mathcal{X}_s)$.

B. Discrete OT and Wasserstein Distance

OT is a mathematical framework that aims to find the optimal transformation from one probability distribution into another by minimizing the associated transportation cost. Moreover, the minimal transportation cost can be interpreted as the distance between the two probability distributions, which is often referred to as the Wasserstein distance [36]–[39]. In the context of localization, OT can be used to align the distribution of estimated positions of users with their true distribution in the environment, thereby improving the overall positioning accuracy [25], [26]. Since this work involves user position samples, we adopt discrete OT and more details on general OT can be found in [36], [37].

Given the source set \mathcal{X}_s and the target set \mathcal{X}_t with $N_s = |\mathcal{X}_s|$ and $N_t = |\mathcal{X}_t|$, we have two defined probability vectors $\mathbf{u}_s \in$

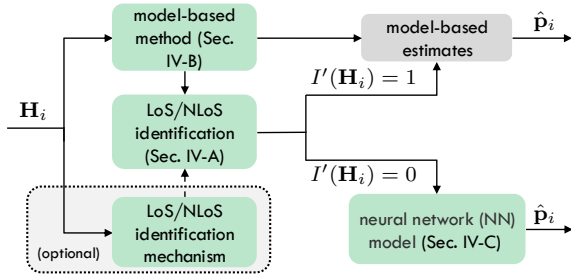


Fig. 2: The framework of UNILocPro (the NN training process is shown in Fig. 3) and UNILoc (the NN training process is shown in Fig. 5).

$\mathbb{R}_+^{N_s \times 1}$ and $\mathbf{u}_t \in \mathbb{R}_+^{N_t \times 1}$ for \mathcal{X}_s and \mathcal{X}_t , respectively, where $[\mathbf{u}_s]_i$ (resp. $[\mathbf{u}_t]_i$) is the probability associated with data sample \mathbf{x}_s^i (resp. \mathbf{x}_t^i). Then, the OT aims to find a transformation from \mathcal{X}_s to \mathcal{X}_t , as denoted by $\mathbf{T}^* : \mathcal{X}_s \rightarrow \mathcal{X}_t$, that minimizes the transportation cost on the condition that the transformation \mathbf{T}^* would push the probability vector \mathbf{u}_s in the source set \mathcal{X}_s toward the probability vector \mathbf{u}_t in the target set \mathcal{X}_t . In particular, the discrete OT problem can be written as [36]

$$\begin{aligned} \mathbf{T}^* = \arg \min_{\mathbf{T}: \mathcal{X}_s \rightarrow \mathcal{X}_t} & \sum_{\mathbf{x}_s^i \in \mathcal{X}_s} c(\mathbf{x}_s^i, \mathbf{T}(\mathbf{x}_s^i)), \\ \text{s.t. } [\mathbf{u}_t]_j = & \sum_{i: \mathbf{T}(\mathbf{x}_s^i) = \mathbf{x}_t^j} [\mathbf{u}_s]_i, \forall \mathbf{x}_t^j \in \mathcal{X}_t, \end{aligned} \quad (4)$$

where $c(\mathbf{x}_s, \mathbf{T}(\mathbf{x}_s))$ is the cost to transform \mathbf{x}_s to $\mathbf{T}(\mathbf{x}_s)$, which can be defined differently for specific applications.

The Kantorovich relaxation of the above problem (4) can be formulated by finding a joint probability matrix $\boldsymbol{\Gamma} \in \mathbb{R}_+^{N_s \times N_t}$ ($[\boldsymbol{\Gamma}]_{i,j}$ is the probability of $(\mathbf{x}_s^i, \mathbf{x}_t^j)$) with marginals \mathbf{u}_s and \mathbf{u}_t to minimize $\sum_{\mathbf{x}_s^i \in \mathcal{X}_s, \mathbf{x}_t^j \in \mathcal{X}_t} c(\mathbf{x}_s^i, \mathbf{x}_t^j) \cdot [\boldsymbol{\Gamma}]_{i,j}$, i.e.,

$$\boldsymbol{\Gamma}^* = \arg \min_{\boldsymbol{\Gamma} \in \mathcal{B}} \langle \boldsymbol{\Gamma}, \mathbf{C} \rangle_F, \quad (5)$$

where $\mathbf{C} \in \mathbb{R}_+^{N_s \times N_t}$ is the transportation cost matrix with $[\mathbf{C}]_{i,j} = c(\mathbf{x}_s^i, \mathbf{x}_t^j)$, and $\mathcal{B} = \{\boldsymbol{\Gamma} \in \mathbb{R}_+^{N_s \times N_t} | \boldsymbol{\Gamma} \cdot \mathbf{1}_{N_t} = \mathbf{u}_s, \boldsymbol{\Gamma}^\top \cdot \mathbf{1}_{N_s} = \mathbf{u}_t\}$. Then, based on the OT problem (5), the Wasserstein distance of order p ($p \geq 1$) between \mathbf{u}_s in \mathcal{X}_s and \mathbf{u}_t in \mathcal{X}_t can be defined as $\mathcal{W}_p(\mathbf{u}_s, \mathbf{u}_t) = \langle \boldsymbol{\Gamma}^*, \mathbf{C} \rangle_F^{\frac{1}{p}}$, where $c(\mathbf{x}_s^i, \mathbf{x}_t^j) = [d(\mathbf{x}_s^i, \mathbf{x}_t^j)]^p$ with $d(\mathbf{x}_s^i, \mathbf{x}_t^j)$ being a distance [36], [37], [40]. It is observed that (5) is a linear programming problem and can be solved by, e.g., simplex methods [37], which usually incur a polynomial time complexity.

IV. UNILOCPRO: UNIFIED LOCALIZATION FRAMEWORK

In this section, we introduce the proposed UNILocPro framework that is illustrated in Fig. 2. Firstly, LoS/NLoS identification is conducted based on CSI \mathbf{H}_i ; then, if user i is identified as a LoS user, the model-based method would be used to estimate its position; otherwise, a NN model is adopted to generate $\hat{\mathbf{p}}_i$ based on \mathbf{H}_i . The model-based and NN-based methods are integrated as

$$\hat{\mathbf{p}}_i = f_e(\mathbf{H}_i) = \begin{cases} f_{pe}[f_{ce}^{sh}(\mathbf{H}_i)], & \text{if } I'(\mathbf{H}_i) = 1; \\ f_\Theta[f_{extr}(\mathbf{H}_i)], & \text{if } I'(\mathbf{H}_i) = 0, \end{cases} \quad (6)$$

where $f_{ce}^{sh}(\cdot)$ is a channel parameter estimation function; $f_{pe}(\cdot)$ is a function that maps channel parameters to position based on geometric relationships; $f_{extr}(\cdot)$ is a channel feature extraction function to transform CSI \mathbf{H}_i to the input of the NN model; $f_\Theta(\cdot)$ is the forward function of the NN model with Θ being parameters; and $I'(\cdot)$ is a CSI-based LoS/NLoS identification

function. Each of the aforementioned functions and blocks is described in detail in the following subsections.

A. LoS/NLoS Identification

CSI-based LoS/NLoS identification has been extensively studied, achieving up to 93%-100% accuracy under various settings [5], [28]. It is assumed that we have a LoS/NLoS identification mechanism, denoted by $I(\cdot)$, where user i is identified as a LoS user if $I(\mathbf{H}_i) = 1$ and as a NLoS user if $I(\mathbf{H}_i) = 0$. For the given $I(\cdot)$, the identification accuracy is denoted by $p_I \in [0.5, 1]$. Furthermore, with a LoS path, the mapping function $f_{pe}(\cdot)$, e.g., solving geometric relationships based on AoA and ToA, would result in a position in the LoS region. This allows us to conclude that all LoS users would be localized in the LoS region with $f_{pe}[f_{ce}^{sh}(\cdot)]$, i.e., if a user is localized in the NLoS region, it must be a NLoS user.³ Therefore, given the results from $I(\mathbf{H}_i)$, we can further improve the LoS/NLoS identification by

$$I'(\mathbf{H}_i) = \begin{cases} 0, & \text{if } f_{pe}[f_{ce}^{sh}(\mathbf{H}_i)] \in \mathcal{R}_{NLoS}; \\ I(\mathbf{H}_i), & \text{if } f_{pe}[f_{ce}^{sh}(\mathbf{H}_i)] \in \mathcal{R}_{LoS}, \end{cases} \quad (7)$$

where $I'(\cdot)$ is the final LoS/NLoS identification function.

Remark: When the mechanism $I(\cdot)$ is not accessible or its identification accuracy p_I drops below some threshold, a conservative method that does not rely on $I(\cdot)$ can be applied. In particular, without $I(\cdot)$, the model-based results could be used for LoS/NLoS identification, i.e., if a user is localized in the LoS (resp. NLoS) region based on $f_{pe}[f_{ce}^{sh}(\cdot)]$, it would be identified as a LoS (resp. NLoS) user. Therefore, the LoS/NLoS identification (7) can be reformulated as

$$I'(\mathbf{H}_i) = \begin{cases} 0, & \text{if } f_{pe}[f_{ce}^{sh}(\mathbf{H}_i)] \in \mathcal{R}_{NLoS}; \\ 1, & \text{if } f_{pe}[f_{ce}^{sh}(\mathbf{H}_i)] \in \mathcal{R}_{LoS}, \end{cases} \quad (8)$$

based on which LoS and NLoS users can be identified completely by $f_{pe}[f_{ce}^{sh}(\mathbf{H}_i)]$.

B. Model-based Localization Method

As discussed in Sec. II-A, the channel estimation algorithm estimates the channel parameters based on \mathbf{H}_i by $\{\hat{\theta}_l^i, \hat{\tau}_l^i, \hat{\beta}_l^i\}_{l=1,2,\dots,\hat{L}_i} = f_{ce}(\mathbf{H}_i)$, where \hat{L}_i is the number of recovered channel paths for user i . For a low complexity implementation, the shortest channel path among the recovered \hat{L}_i paths is identified as the LoS path and used to estimate the user position. Thus, the channel parameter estimation function $f_{ce}^{sh}(\cdot)$ that maps the CSI to AoA and ToA can be written as $\{\hat{\theta}_s^i, \hat{\tau}_s^i\} = f_{ce}^{sh}(\mathbf{H}_i)$, $\forall i$, where $s = \arg \min_l \hat{\tau}_l^i$, $l = 1, 2, \dots, \hat{L}_i$. Then, with AoA and ToA, the user position estimate can be derived based on geometric relationships [3], [5], [6], [8]. In particular, the model-based estimate $\hat{\mathbf{p}}_i^{mb}$ can be written as $\hat{\mathbf{p}}_i^{mb} = f_{pe}[f_{ce}^{sh}(\mathbf{H}_i)]$, $\forall i$, where $f_{pe}(\cdot)$ is obtained by solving the geometric relationships between the user position and the channel parameters [1], [3], [5].

C. CC-based Localization Method

In order to obtain a parametric CC model, NN is adopted to map CSI to position.⁴ In order to reduce the dimension of input and also make NN easier to learn hidden patterns, CSI

³However, NLoS users could be localized in LoS region by $f_{pe}[f_{ce}^{sh}(\cdot)]$ due to reflection, diffraction, or scattering of the physical environment.

⁴In our implementation, an L_{MLP} -layer multi-layer perceptron (MLP) with layer widths $\{n_l\}_{l=1,\dots,L_{MLP}}$ is adopted for the NN model (we also use n_0 to denote the dimensionality of \mathbf{s}_i).

preprocessing is adopted [12], [17]. We first convert the antenna-frequency domain CSI \mathbf{H}_i to the angle-delay domain, i.e., $\bar{\mathbf{H}}_i = \mathcal{F}_a[\mathcal{F}_b^{-1}(\mathbf{H}_i)]$, $\forall i$, where $\mathcal{F}_a(\cdot)$ is the discrete Fourier transform along the antenna axis and $\mathcal{F}_b^{-1}(\cdot)$ is the inverse discrete Fourier transform along the frequency axis. Then, $\bar{\mathbf{H}}_i$ can be truncated by taking the columns that have delays within the minimum ToA τ_{\min} and the maximum ToA τ_{\max} . Specifically, we truncate $\bar{\mathbf{H}}_i$ as $\bar{\mathbf{H}}_i^t = [\bar{\mathbf{H}}_i]_{:, \lfloor \tau_{\min} \Delta_f N_c \rfloor : \lceil \tau_{\max} \Delta_f N_c \rceil}$, $\forall i$, whose element-wise amplitude and phase are used to generate the input to the NN [12], [14], [22], as denoted by $\mathbf{s}_i = \text{vec}([\log(|\bar{\mathbf{H}}_i^t|), \angle \bar{\mathbf{H}}_i^t])$, $\forall i$. Thus, implementing CSI domain conversion, truncation, and element-wise extraction, $f_{\text{extr}}(\cdot)$ transforms \mathbf{H}_i to the input of the NN model, i.e., $\mathbf{s}_i = f_{\text{extr}}(\mathbf{H}_i)$, based on which the output of the NN model, i.e., the user position estimate $\hat{\mathbf{p}}_i^{\text{nb}}$, can be expressed by $\hat{\mathbf{p}}_i^{\text{nb}} = f_{\Theta}[f_{\text{extr}}(\mathbf{H}_i)]$, $\forall i$.

Given a dataset $\mathcal{S} = \{\mathbf{H}_i, \mathbf{p}_i\}_{i=1,2,\dots,N_u}$, where N_u is the number of user positions, the ground-truth positions $\{\mathbf{p}_i\}$ are not available for training but only for validation since unsupervised learning is aimed for in this paper.⁵ Then, by executing $\mathbf{s}_i = f_{\text{extr}}(\mathbf{H}_i)$ and $I'(\mathbf{H}_i)$ in (7) or (8), the dataset \mathcal{S} can be transformed to $\mathcal{S}' = \{\mathbf{s}_i, I'(\mathbf{H}_i)\}_{i=1,2,\dots,N_u}$ (the ground-truth positions $\{\mathbf{p}_i\}$ are not included), which can be used to update the parameters Θ through backpropagation by minimizing an overall CC loss function (as shown in Fig. 3):

$$\mathcal{L}_{\text{CC}} = \omega_{\text{C-CC}} \cdot \mathcal{L}_{\text{C-CC}} + \omega_{\text{LoS}} \cdot \mathcal{L}_{\text{LoS}} + \omega_{\text{OT}} \cdot \mathcal{L}_{\text{OT}}, \quad (9)$$

where $\mathcal{L}_{\text{C-CC}}$ is the conventional CC loss [14], [15], which generates a channel chart that preserves local geometry; \mathcal{L}_{LoS} is the LoS-based loss, which aligns the channel chart with the global coordinates by using identified LoS users as anchors and also improves their localization accuracy; \mathcal{L}_{OT} is the map-assisted loss (computed based on OT), which constrains the estimated positions of identified NLoS users in the NLoS region (these losses will be detailed in Sec. V); These losses are weighted by positive coefficients $\omega_{\text{C-CC}}$, ω_{LoS} , and ω_{OT} , respectively, which can be tuned according to specific applications and datasets to balance their contributions. Therefore, these losses are complementary to each other and jointly optimized to achieve robust localization performance.

V. MULTI-COMPONENT CC LOSS

In this section, we present each loss term in the overall CC loss \mathcal{L}_{CC} in (9) and the proposed dissimilarity metrics.

A. Conventional CC Loss

In the literature, the conventional CC loss functions usually contain the pairwise distance loss \mathcal{L}_{PWD} and the triplet loss \mathcal{L}_{Tri} , based on which $\mathcal{L}_{\text{C-CC}}$ can be written as [14], [15]

$$\mathcal{L}_{\text{C-CC}} = \omega_{\text{PWD}} \mathcal{L}_{\text{PWD}} + \omega_{\text{Tri}} \mathcal{L}_{\text{Tri}}, \quad (10)$$

where ω_{PWD} and ω_{Tri} are non-negative coefficients. The pairwise distance loss, which is a contrastive loss function, is effective in learning the relationships between pairs of CSI samples [14], [16], [17], [19], [22], where the main idea is that the distance between two CSI samples should be preserved in the channel chart. In particular, the pairwise distance loss

⁵We use “user positions” instead of “users” since the CSIs in the dataset \mathcal{S} could be from multiple users at different positions, i.e., the same user could have multiple CSIs at different positions.

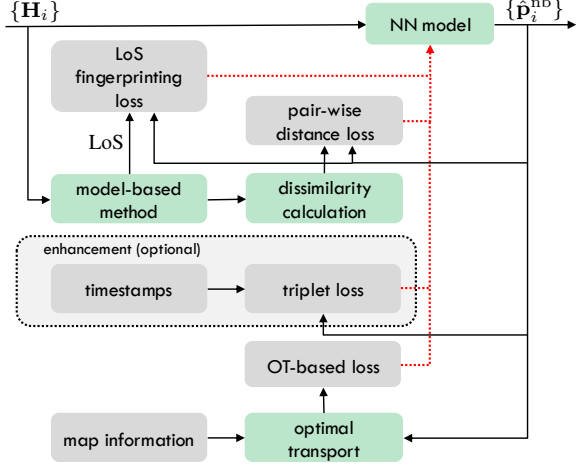


Fig. 3: The training process of the NN model in UNILocPro (the red dashed arrow line indicates the path of gradient backpropagation).

\mathcal{L}_{PWD} that preserves the distance $d_{i,j} = d(\mathbf{H}_i, \mathbf{H}_j)$ can be written as [17]

$$\mathcal{L}_{\text{PWD}} = \frac{1}{N_u^2} \sum_{\mathbf{s}_i \in \mathcal{S}'} \sum_{\mathbf{s}_j \in \mathcal{S}'} \frac{(\|\mathbf{f}_{\Theta}(\mathbf{s}_i) - \mathbf{f}_{\Theta}(\mathbf{s}_j)\|_2 - d_{i,j})^2}{d_{i,j}}. \quad (11)$$

As for the triplet loss [15], [41], given dissimilarity metric $d(\cdot, \cdot)$, a triplet $(\mathbf{H}_p, \mathbf{H}_n, \mathbf{H}_r)$ in the triplet set $\mathcal{T} \subseteq \mathcal{S}^3$ contains a reference sample \mathbf{H}_r , a positive sample \mathbf{H}_p , and a negative sample \mathbf{H}_n , such that the positive sample is closer to the reference sample than the negative sample, i.e., $d(\mathbf{H}_r, \mathbf{H}_p) < d(\mathbf{H}_r, \mathbf{H}_n)$. Therefore, the triplet set \mathcal{T} can be defined as

$$\mathcal{T} = \left\{ (\mathbf{H}_p, \mathbf{H}_n, \mathbf{H}_r) \mid \begin{array}{l} 0 \leq d(\mathbf{H}_r, \mathbf{H}_p) \leq d_L \\ d_L < d(\mathbf{H}_r, \mathbf{H}_n) \leq d_U \end{array} \right\}, \quad (12)$$

where d_L and d_U are parameters. When training the NN model $f_{\Theta}(\cdot)$, the distance relationship of the triplet samples from the triplet set \mathcal{T} can be enforced in the channel chart, i.e., $\|\hat{\mathbf{p}}_p^{\text{nb}} - \hat{\mathbf{p}}_r^{\text{nb}}\|_2 < \|\hat{\mathbf{p}}_n^{\text{nb}} - \hat{\mathbf{p}}_r^{\text{nb}}\|_2$, by the triplet loss (13), where $\gamma > 0$ is a margin parameter.

For localization, it is desired that the distance $d(\mathbf{H}_i, \mathbf{H}_j)$ is the physical distance between user positions, i.e., $d(\mathbf{H}_i, \mathbf{H}_j) = \|\mathbf{p}_i - \mathbf{p}_j\|_2$, which however is not directly accessible since supervision is not available. In practice, it is challenging to design a metric that is consistent with the physical distance based solely on CSI, i.e., only relying on manipulations on CSI. In this paper, as one of our main contributions, we propose two different metrics (as well as their fusion) based on the GOSPA metric and the Wasserstein distance, which could serve as approximations of the physical distance and thus achieve good CC and localization performance.

With the estimated channel parameters of the \hat{L}_i recovered channel paths $\{\hat{\beta}_l^i, \hat{\theta}_l^i, \hat{\tau}_l^i\} = f_{\text{ce}}(\mathbf{H}_i)$ from the CSI \mathbf{H}_i , \hat{L}_i positions can be generated for \mathbf{H}_i via the channel parameters-to-position function $f_{\text{pe}}(\cdot)$, as denoted by $\{\hat{\mathbf{p}}_{i,l}^{\text{mb}}\}_{l=1,\dots,\hat{L}_i}$ (can be regarded as a signature of \mathbf{H}_i), where $\hat{\mathbf{p}}_{i,l}^{\text{mb}} = f_{\text{pe}}(\{\hat{\beta}_l^i, \hat{\theta}_l^i\})$ is the model-based position estimate for the l -th channel path of \mathbf{H}_i . Here, we treat every path as LoS to compute a coarse estimate, which serves not as an accurate location, but as a geometric surrogate that can be used for dissimilarity computations. Then, the dissimilarity metric $d(\mathbf{H}_i, \mathbf{H}_j)$ can

$$\mathcal{L}_{\text{Tri}} = \frac{1}{|\mathcal{T}|} \sum_{(\mathbf{H}_p, \mathbf{H}_n, \mathbf{H}_r) \in \mathcal{T}} \max(0, \|f_{\Theta}[f_{\text{extr}}(\mathbf{H}_p)] - f_{\Theta}[f_{\text{extr}}(\mathbf{H}_r)]\|_2 - \|f_{\Theta}[f_{\text{extr}}(\mathbf{H}_n)] - f_{\Theta}[f_{\text{extr}}(\mathbf{H}_r)]\|_2 + \gamma). \quad (13)$$

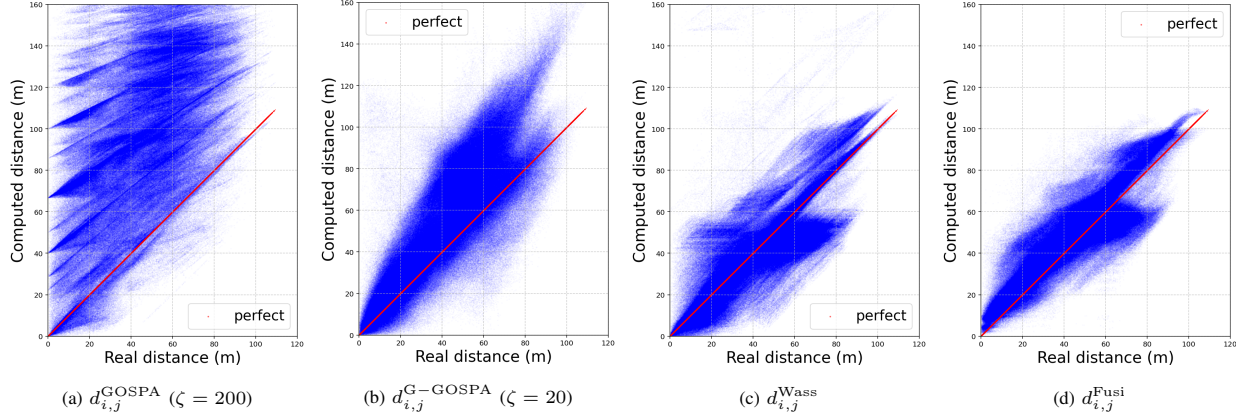


Fig. 4: The computed dissimilarity v.s. the physical distance between user positions, where the red line represents the real distance (using the same system setting as described in Sec. VII-A).

be designed as the distance between the sets of positions $\{\hat{\mathbf{p}}_{i,l}^{\text{mb}}\}_{l=1, \dots, \hat{L}_i}$ and $\{\hat{\mathbf{p}}_{j,l}^{\text{mb}}\}_{l=1, \dots, \hat{L}_j}$, as written by

$$d(\mathbf{H}_i, \mathbf{H}_j) = \mathcal{D}\left(\{\hat{\mathbf{p}}_{i,l}^{\text{mb}}\}_{l=1, \dots, \hat{L}_i}, \{\hat{\mathbf{p}}_{j,l}^{\text{mb}}\}_{l=1, \dots, \hat{L}_j}\right), \quad (14)$$

where $\mathcal{D}(\cdot, \cdot)$ is a metric that measures the dissimilarity between two sets of positions. In this paper, we propose using the GOSPA metric and the Wasserstein distance as $\mathcal{D}(\cdot, \cdot)$, both of which are effective for measuring the dissimilarity between sets of points.

1) GOSPA-Based Dissimilarity

As one of the metrics between two sets of points, the GOSPA metric (3) with $p = 1$, $\varpi = 2$, and $d(\mathbf{x}, \mathbf{y}) = \|\mathbf{x} - \mathbf{y}\|_2$ can be used for $d(\mathbf{H}_i, \mathbf{H}_j)$ to indicate the physical distance, i.e.,

$$d_{i,j}^{\text{GOSPA}} = \frac{\mathcal{G}_1^{(\zeta, 2)}(\{\hat{\mathbf{p}}_{i,l}^{\text{mb}}\}_{l=1, \dots, \hat{L}_i}, \{\hat{\mathbf{p}}_{j,l}^{\text{mb}}\}_{l=1, \dots, \hat{L}_j})}{(\hat{L}_i + \hat{L}_j)/2}, \quad (15)$$

where a normalization is applied such that $d_{i,j}^{\text{GOSPA}}$ has the scale of the physical distance between a pair of positions. As shown in Fig. 4, directly using $d_{i,j}^{\text{GOSPA}}$ by setting the cut-off value ζ be a large value is not appropriate since reflection, diffraction, and/or scattering may bias the GOSPA metric. For example, for two user positions that are close to each other, some pairs of positions from $\{\hat{\mathbf{p}}_{i,l}^{\text{mb}}\}_{l=1, \dots, \hat{L}_i}$ and $\{\hat{\mathbf{p}}_{j,l}^{\text{mb}}\}_{l=1, \dots, \hat{L}_j}$ (one position from $\{\hat{\mathbf{p}}_{i,l}^{\text{mb}}\}_{l=1, \dots, \hat{L}_i}$ and the other one from $\{\hat{\mathbf{p}}_{j,l}^{\text{mb}}\}_{l=1, \dots, \hat{L}_j}$) can be very far away due to reflection, diffraction, and/or scattering. Therefore, in order to have a better representation, we can set ζ to be a relatively small value and use the geodesic dissimilarity [17], [22] based on $\{d_{i,j}^{\text{GOSPA}}\}$ to compute the geodesic GOSPA metric as

$$d_{i,j}^{\text{G-GOSPA}} = \sum_{k \in \mathcal{P}_{i,j}} d(\mathbf{H}_k, \mathbf{H}_{k+1}) = \sum_{k \in \mathcal{P}_{i,j}} d_{k,k+1}^{\text{GOSPA}}, \quad (16)$$

where k and $k+1$ are the indices of all neighboring pairs of points on the shortest path $\mathcal{P}_{i,j}$ between \mathbf{H}_i and \mathbf{H}_j , which can be obtained by utilizing shortest path algorithms, e.g., Dijkstra's algorithm, on the neighbor graphs constructed from $\{d_{i,j}^{\text{GOSPA}}\}$. More details about the geodesic dissimilarity can be found in [17], [22]. As shown in Fig. 4, the geodesic GOSPA metric $d_{i,j}^{\text{G-GOSPA}}$ is more consistent with the physical distance than the GOSPA metric $d_{i,j}^{\text{GOSPA}}$.

2) Wasserstein-Based Dissimilarity

As the Wasserstein distance is a metric that measures the dissimilarity between two probability distributions, it can also be used as $\mathcal{D}(\cdot, \cdot)$ when probability distributions are defined for the sets of positions $\{\hat{\mathbf{p}}_{i,l}^{\text{mb}}\}_{l=1, \dots, \hat{L}_i}$ and $\{\hat{\mathbf{p}}_{j,l}^{\text{mb}}\}_{l=1, \dots, \hat{L}_j}$. Then, our next task is to construct a spatial probability distribution, denoted by \mathbf{u}_i , for each set of positions $\{\hat{\mathbf{p}}_{i,l}^{\text{mb}}\}_{l=1, \dots, \hat{L}_i}$, $\forall i$. To do so, we can assign a probability mass to each recovered position in $\{\hat{\mathbf{p}}_{i,l}^{\text{mb}}\}_{l=1, \dots, \hat{L}_i}$, $\forall i$, based on the reliability of its underlying estimated channel parameters $\{\hat{\beta}_l^i, \hat{\theta}_l^i, \hat{\tau}_l^i\}$, which can be written as

$$[\mathbf{u}_i]_l = p(\hat{\beta}_l^i, \hat{\theta}_l^i, \hat{\tau}_l^i), \quad \forall l, \quad (17)$$

where $p(\cdot)$ is a probability mass function. In particular, being key indicators of reliability, channel gain $\hat{\beta}_l^i$ and ToA $\hat{\tau}_l^i$ are utilized in this paper. In general, stronger channel paths are typically estimated with higher accuracy and are more likely to represent genuine physical geometry. Furthermore, the LoS path and the earliest NLoS path are often the most geometrically reliable. Therefore, we aim to assign higher probability to paths that have high energy and arrive early, prioritizing the most stable and geometrically informative components of the channel. As the channel paths that arrive early are usually with higher channel gains, being an example implementation, we simply use

$$p(\hat{\beta}_l^i, \hat{\theta}_l^i, \hat{\tau}_l^i) = \frac{\exp(-\kappa\hat{\tau}_l^i)}{\sum_l \exp(-\kappa\hat{\tau}_l^i)}, \quad \forall l, \quad (18)$$

where $\kappa > 0$ is a parameter and can be chosen empirically.

Given $\{\hat{\mathbf{p}}_{i,l}^{\text{mb}}\}_{l=1, \dots, \hat{L}_i}$ and $\{\hat{\mathbf{p}}_{j,l}^{\text{mb}}\}_{l=1, \dots, \hat{L}_j}$, the first-order Wasserstein distance between \mathbf{u}_i and \mathbf{u}_j can be used as the dissimilarity metric $d(\mathbf{H}_i, \mathbf{H}_j)$, which is written as

$$d_{i,j}^{\text{Wass}} = \min_{\mathbf{\Gamma} \in \mathcal{B}} \langle \mathbf{\Gamma}, \mathbf{C} \rangle_F, \quad (19)$$

where $\mathbf{C} \in \mathbb{R}_{+}^{\hat{L}_i \times \hat{L}_j}$ with $[\mathbf{C}]_{l,l'} = \|\hat{\mathbf{p}}_{i,l}^{\text{mb}} - \hat{\mathbf{p}}_{j,l'}^{\text{mb}}\|_2$; and $\mathcal{B} = \{\mathbf{\Gamma} \in \mathbb{R}_{+}^{\hat{L}_i \times \hat{L}_j} \mid \mathbf{\Gamma} \cdot \mathbf{1}_{\hat{L}_j} = \mathbf{u}_i, \mathbf{\Gamma}^T \cdot \mathbf{1}_{\hat{L}_i} = \mathbf{u}_j\}$. As shown in Fig. 4, unlike the GOSPA metric $d_{i,j}^{\text{GOSPA}}$, the Wasserstein distance $d_{i,j}^{\text{Wass}}$ can represent the physical distance and thus using the geodesic dissimilarity is not necessary in this case.

3) Dissimilarity Fusion

In addition to the GOSPA-based and Wasserstein-based dissimilarity metrics, we can also fuse these two metrics to achieve a better dissimilarity metric. Before fusion, we first explore these two dissimilarity metrics numerically such that a proper fusion strategy can be designed. The computed dissimilarity metrics $d_{i,j}^{\text{G-GOSPA}}$ and $d_{i,j}^{\text{Wass}}$ are shown in Fig. 4, where it can be observed that $d_{i,j}^{\text{G-GOSPA}}$ is more consistent when the physical distance is small, while $d_{i,j}^{\text{Wass}}$ is more consistent when the physical distance is large. Therefore, to blend the complementary benefits of the two approaches, we can fuse the GOSPA-based and Wasserstein-based metrics by

$$d_{i,j}^{\text{Fusi}} = \alpha_{i,j} \cdot d_{i,j}^{\text{G-GOSPA}} + (1 - \alpha_{i,j}) \cdot d_{i,j}^{\text{Wass}}, \quad (20)$$

where $\alpha_{i,j} \in [0, 1]$ is a coefficient. Aiming to have a large $\alpha_{i,j}$ when $d_{i,j}^{\text{G-GOSPA}}$ is small, while a small $\alpha_{i,j}$ when $d_{i,j}^{\text{Wass}}$ is large, we adopt the following method to compute $\alpha_{i,j}$ in our implementation:

$$\alpha_{i,j} = \begin{cases} 1, & \text{if } d_{i,j}^{\text{G-GOSPA}} \leq d_{\text{thre}}; \\ (1 + \vartheta \cdot d_{i,j}^{\text{G-GOSPA}})^{-1}, & \text{if } d_{i,j}^{\text{G-GOSPA}} > d_{\text{thre}}, \end{cases} \quad (21)$$

where $\vartheta \geq 0$ and $d_{\text{thre}} \geq 0$ are prespecified parameters.

4) Timestamps

When timestamps are available for CSI measurements, they indicate the time difference between CSIs, which can be exploited to enhance CC and localization performance [15], [17], [41]. For a trajectory \mathcal{S}_{tr} , each CSI measurement \mathbf{H}_i is associated with a position \mathbf{p}_i and a timestamp t_i , i.e., $\mathcal{S}_{\text{tr}} = \{\mathbf{H}_i, \mathbf{p}_i, t_i\}$. Intuitively, the time difference between two CSIs can be used as a dissimilarity metric [17]:

$$d_{i,j}^{\text{time}} = |t_i - t_j|, \quad \forall t_i, t_j \in \mathcal{S}_{\text{tr}}. \quad (22)$$

However, $d_{i,j}^{\text{time}}$ becomes unreliable for large time gaps, limiting CC performance if directly applied in the pairwise distance loss \mathcal{L}_{PWD} (11) (as shown by $d_{i,j}^{\text{time}}$ (\mathcal{L}_{PWD}) in Table I). Instead, it can be used to construct triplet sets for training [15], [41]. Specifically, based on $\{d_{i,j}^{\text{time}}\}$, the triplet set $\mathcal{T}_{\text{tr}} \subseteq \mathcal{S}_{\text{tr}}^3$ can be defined as

$$\mathcal{T}_{\text{tr}} = \{(\mathbf{H}_p, \mathbf{H}_n, \mathbf{H}_r)\} \subseteq \mathcal{S}_{\text{tr}}^3, \quad (23)$$

where $0 \leq |t_p - t_r| \leq T_{\text{L}} < |t_n - t_r| \leq T_{\text{U}}$ with T_{L} and T_{U} being parameters. Then, the corresponding triplet loss can be obtained by summing over all trajectories as defined in (13).

B. LoS-Based Loss

Since precise position estimates can be obtained by model-based methods for LoS users, a loss term corresponding to the estimation accuracy of the identified LoS user positions, i.e., \mathcal{L}_{LoS} in (9), is designed as

$$\mathcal{L}_{\text{LoS}} = \frac{1}{\sum_i I'(\mathbf{H}_i)} \sum_{\{\mathbf{s}_i | I'(\mathbf{H}_i) = 1\}} \|f_{\Theta}(\mathbf{s}_i) - \hat{\mathbf{p}}_i^{\text{mb}}\|_2^2. \quad (24)$$

Note that \mathcal{L}_{LoS} is only applied to the identified LoS user positions, i.e., when $I'(\mathbf{H}_i) = 1$, which encourages the NN model to learn the mapping from CSI to position for LoS users, leveraging the accurate model-based estimates as supervision. This is critical for CC to preserve the global geometry as the model-based estimates for identified LoS users are used as anchor locations such that the generated channel chart can match the global coordinates during training.

C. OT-based Loss

For identified LoS user positions, it can be seen that the position estimate $\hat{\mathbf{p}}_i^{\text{nb}} = f_{\Theta}[f_{\text{extr}}(\mathbf{H}_i)]$ from the NN model is in the LoS region, i.e., $\hat{\mathbf{p}}_i^{\text{nb}} \in \mathcal{R}_{\text{LoS}}$, since the LoS-based loss \mathcal{L}_{LoS} (24) is adopted, where $\hat{\mathbf{p}}_i^{\text{mb}} = f_{\text{pe}}[f_{\text{ce}}^{\text{sh}}(\mathbf{H}_i)] \in \mathcal{R}_{\text{LoS}}$ (minimizing \mathcal{L}_{LoS} (24) provides $f_{\Theta}[f_{\text{extr}}(\mathbf{H}_i)] = \hat{\mathbf{p}}_i^{\text{mb}}$). However, for identified NLoS user positions, the position estimate $\hat{\mathbf{p}}_i^{\text{nb}}$ is not necessarily in the NLoS region, i.e., $\hat{\mathbf{p}}_i^{\text{nb}} \notin \mathcal{R}_{\text{NLoS}}$ for some user positions. With the map information, it is known that all NLoS user positions should be in the NLoS region, and therefore the OT-based loss \mathcal{L}_{OT} can be introduced to ensure that the position estimates $\hat{\mathbf{p}}_i^{\text{nb}}$ for identified NLoS user positions are in the NLoS region, i.e., $\hat{\mathbf{p}}_i^{\text{nb}} \in \mathcal{R}_{\text{NLoS}}$ if $I'(\mathbf{H}_i) = 0, \forall i$.

In particular, when resorting to OT (5), we sample N_t (proportional to $N_s = N_u - \sum_i I'(\mathbf{H}_i)$) candidate user positions in the NLoS region according to the PDF of user distribution $f_{\text{D}}^{\text{NLoS}}(\cdot)$ in (2), yielding a user position set $\{\bar{\mathbf{p}}_i\}_{i=1,2,\dots,N_t}$, where each position $\bar{\mathbf{p}}_i$ is drawn i.i.d. from the distribution:

$$\bar{\mathbf{p}}_i \stackrel{\text{i.i.d.}}{\sim} f_{\text{D}}^{\text{NLoS}}(\mathbf{p}), \quad i = 1, \dots, N_t. \quad (25)$$

Then, in the OT problem (5), we can let the source set $\mathcal{X}_s = \{\hat{\mathbf{p}}_i^{\text{nb}} | I'(\mathbf{H}_i) = 0\}_{i=1,2,\dots,N_u}$, the target set $\mathcal{X}_t = \{\bar{\mathbf{p}}_i\}_{i=1,2,\dots,N_t}$, the probability vector $\mathbf{u}_s = \frac{1}{N_s} \cdot \mathbf{1}_{N_s}$ (for user positions in the source set \mathcal{X}_s) and the probability vector $\mathbf{u}_t = \frac{1}{N_t} \cdot \mathbf{1}_{N_t}$ (for user positions in the target set \mathcal{X}_t). Based on the source set \mathcal{X}_s , the target set \mathcal{X}_t , and their position probability vectors \mathbf{u}_s and \mathbf{u}_t , the OT-based loss \mathcal{L}_{OT} can be designed as the first-order Wasserstein distance, which can be written as

$$\mathcal{L}_{\text{OT}} = \mathcal{W}_1(\mathbf{u}_s, \mathbf{u}_t) = \min_{\mathbf{\Gamma} \in \mathcal{B}} \langle \mathbf{\Gamma}, \mathbf{C} \rangle_F = \langle \mathbf{\Gamma}^*, \mathbf{C} \rangle_F, \quad (26)$$

where the cost associated with two positions is set as the Euclidean distance, i.e., $[\mathbf{C}]_{i',j} = \|\hat{\mathbf{p}}_i^{\text{nb}} - \bar{\mathbf{p}}_j\|_2$.⁶

1) Loss Computation

Therefore, by minimizing the OT-based loss \mathcal{L}_{OT} during training, the position estimates $\{\hat{\mathbf{p}}_i^{\text{nb}} | I'(\mathbf{H}_i) = 0\}$ can be aligned with the sampled positions $\{\bar{\mathbf{p}}_i\}$, which gives $\hat{\mathbf{p}}_i^{\text{nb}} = f_{\Theta}[f_{\text{extr}}(\mathbf{H}_i)] \in \mathcal{R}_{\text{NLoS}}$ for $I'(\mathbf{H}_i) = 0$. Note that the estimates $\{\hat{\mathbf{p}}_i^{\text{nb}} | I'(\mathbf{H}_i) = 1\}$ for identified LoS user positions are not included in the OT (26) since they will not be transported and hence have no impact on the OT-based loss. It is clear that \mathcal{L}_{OT} involves an OT optimization problem, which can be shown to be differentiable with respect to the parameters Θ of the NN model by utilizing convex optimization layers [42]–[44]. Specifically, we can define a convex optimization layer $f_{\text{CL}}(\cdot)$, which takes the output of the NN model $\{f_{\Theta}(\mathbf{s}_i) | I'(\mathbf{H}_i) = 0\}_{i=1,2,\dots,N_s}$ as input. The output of the layer $f_{\text{CL}}(\cdot)$ is $\mathbf{\Gamma}^* = f_{\text{CL}}(\{f_{\Theta}(\mathbf{s}_i) | I'(\mathbf{H}_i) = 0\})$, where $\mathbf{\Gamma}^*$ is from (26) with $[\mathbf{C}]_{i',j} = \|f_{\Theta}(\mathbf{s}_i) - \bar{\mathbf{p}}_j\|_2$. It can be seen that $\langle \mathbf{\Gamma}^*, \mathbf{C} \rangle_F$ is differentiable w.r.t. $\mathbf{\Gamma}^*$ and \mathbf{C} ; and \mathbf{C} is differentiable w.r.t. $\{f_{\Theta}(\mathbf{s}_i)\}$. Also, it can be proved that the output of convex optimization layers, i.e., the optimal solution of the corresponding optimization problem, is differentiable w.r.t. the input of the layer [42], [43] (i.e., $\mathbf{\Gamma}^*$ is differentiable w.r.t. $\{f_{\Theta}(\mathbf{s}_i) | I'(\mathbf{H}_i) = 0\}$), based on which we

⁶The i' -th data sample in $\{\hat{\mathbf{p}}_i^{\text{nb}} | I'(\mathbf{H}_i) = 0\}_{i=1,2,\dots,N_u}$ is the i -th data sample in $\{\hat{\mathbf{p}}_i^{\text{nb}}\}_{i=1,2,\dots,N_u}$.

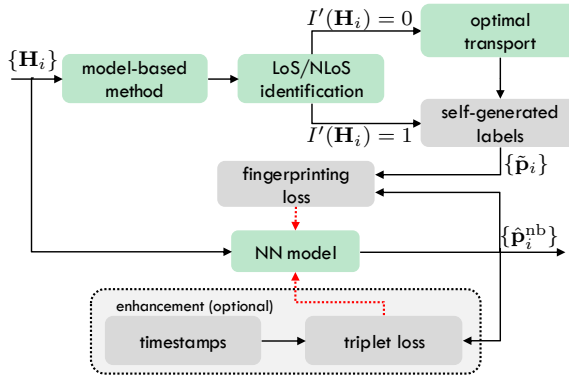


Fig. 5: The training process of the NN model in UNILoc (the red dashed line indicates the path of gradient backpropagation).

can conclude that $\mathcal{L}_{\text{OT}} = \langle \Gamma^*, \mathbf{C} \rangle_F$ is differentiable w.r.t. the parameters Θ since $f_\Theta(\mathbf{s}_i)$ is differentiable w.r.t. Θ . Moreover, the forward pass of $f_{\text{CL}}(\cdot)$ can be implemented by solving (26), and its gradients w.r.t. $\{f_\Theta(\mathbf{s}_i) | I'(\mathbf{H}_i) = 0\}$ can be computed by differentiating its Karush-Kuhn-Tucker (KKT) conditions according to the implicit function theorem [43], based on which the backpropagation of \mathcal{L}_{OT} can be performed through this layer and the NN model w.r.t. Θ . More details about the convex optimization layers can be found in [42]–[44].

2) Sinkhorn Iteration

However, training the NN model directly using $\Gamma^* = f_{\text{CL}}(\{f_\Theta(\mathbf{s}_i) | I'(\mathbf{H}_i) = 0\})$ would require very high computational complexity (prohibitive for large-scale datasets). For example, its training complexity is $\mathcal{O}(N_u \sum_{l=1}^{L_{\text{MLP}}} n_{l-1} n_l + N_u^3 N_t^3)$ per epoch for an L_{MLP} -layer MLP, where $\mathcal{O}(N_u^3 N_t^3)$ is induced by convex optimization layers [44]. Instead, we can use the Sinkhorn algorithm to approximately compute \mathcal{L}_{OT} in a more efficient and differentiable manner [38], [45], [46]. In particular, by adding a regularization term to the OT problem, \mathcal{L}_{OT} can be reformulated as

$$\mathcal{L}_{\text{OT}} = \min_{\Gamma \in \mathcal{B}} \langle \Gamma, \mathbf{C} \rangle_F - \frac{1}{\varepsilon} E(\Gamma), \quad (27)$$

where $E(\Gamma) = -\sum_{i,j} [\Gamma]_{i,j} \log([\Gamma]_{i,j})$ is the entropy term, and $\varepsilon > 0$ is a regularization parameter. It can be proved that (27) is strongly convex and admits an optimal solution, as given by [38], [45]

$$\Gamma^* = \text{diag}(\mathbf{a}) \cdot \exp(-\varepsilon \mathbf{C}) \cdot \text{diag}(\mathbf{b}), \quad (28)$$

where $\mathbf{a} \in \mathbb{R}_+^{N_u \times 1}$ and $\mathbf{b} \in \mathbb{R}_+^{N_t \times 1}$ can be iteratively updated by

$$\mathbf{a} \leftarrow \mathbf{u}_s \oslash [\exp(-\varepsilon \mathbf{C}) \cdot \mathbf{b}], \quad \mathbf{b} \leftarrow \mathbf{u}_t \oslash [\exp(-\varepsilon \mathbf{C})^\top \cdot \mathbf{a}], \quad (29)$$

until convergence. Therefore, by adopting I_{Iter} iterations in (29), \mathcal{L}_{OT} can be computed approximately, which is also differentiable with respect to the parameters Θ since the Sinkhorn update (29) is differentiable. In this case, the training complexity is $\mathcal{O}(N_u \sum_{l=1}^{L_{\text{MLP}}} n_{l-1} n_l + I_{\text{Iter}} N_u N_t)$ per epoch for an L_{MLP} -layer MLP, which is much lower than that of the training using the convex optimization layers.

VI. UNILOC: A LOW-COMPLEXITY APPROACH

In UNILocPro, the Sinkhorn algorithm needs to be performed to compute the OT-based loss \mathcal{L}_{OT} and the backpropagation then traces back through the Sinkhorn iterations in each epoch during training, which could be computationally expensive, especially for very large-scale datasets. In this section, we

introduce UNILoc, a low-complexity approach that can achieve performance comparable to UNILocPro with much lower complexity for the NN model training. Similarly to UNILocPro, the model-based and NN-based methods are integrated as (6), while the NN model is trained using self-generated training labels $\{\tilde{\mathbf{p}}_i\}$ with optional enhancement by timestamps, as shown in Fig. 5. Note that the self-generated labels $\{\tilde{\mathbf{p}}_i\}$ are obtained from the model-based estimates $\{\hat{\mathbf{p}}_i^{\text{mb}}\}$ by applying the OT once, which eliminates the need for the OT at each epoch, thus significantly reducing the training complexity.

A. Self-generated Labels

Given the CSI dataset $\{\mathbf{H}_i\}_{i=1,2,\dots,N_u}$, position estimates $\{\hat{\mathbf{p}}_i^{\text{mb}}\}_{i=1,2,\dots,N_u}$ can be attained based on the model-based method $\hat{\mathbf{p}}_i^{\text{mb}} = f_{\text{pe}}[f_{\text{ce}}^{\text{sh}}(\mathbf{H}_i)]$. For identified LoS user positions, $\{\hat{\mathbf{p}}_i^{\text{mb}}\}$ can be used as training labels, i.e., $\tilde{\mathbf{p}}_i = \hat{\mathbf{p}}_i^{\text{mb}}$ if $I'(\mathbf{H}_i) = 1$; however, these estimates $\hat{\mathbf{p}}_i^{\text{mb}}$ may not be accurate for identified NLoS user positions and do not match the map. Therefore, we aim to find a transformation $\mathbf{T}^*(\cdot)$ that maps $\{\hat{\mathbf{p}}_i^{\text{mb}} | I'(\mathbf{H}_i) = 0\}_{i=1,2,\dots,N_u}$ to some other positions that can match the NLoS region on the map.

To achieve this goal, we resort to the discrete OT in (5), where we let the source set $\mathcal{X}_s = \{\hat{\mathbf{p}}_i^{\text{mb}} | I'(\mathbf{H}_i) = 0\}_{i=1,2,\dots,N_u}$ and the target set $\mathcal{X}_t = \{\tilde{\mathbf{p}}_i\}_{i=1,2,\dots,N_t}$, where $\{\tilde{\mathbf{p}}_i\}_{i=1,2,\dots,N_t}$ is a set of candidate user positions in the NLoS region sampled according to the PDF of user distribution $f_D^{\text{NLoS}}(\cdot)$, as given in (25). Moreover, by setting $[\mathbf{C}]_{i',j} = \|\hat{\mathbf{p}}_i^{\text{mb}} - \tilde{\mathbf{p}}_j\|_2^2$, $\mathbf{u}_s = \frac{1}{N_s} \cdot \mathbf{1}_{N_s}$, and $\mathbf{u}_t = \frac{1}{N_t} \cdot \mathbf{1}_{N_t}$, the joint probability matrix $\Gamma \in \mathbb{R}_+^{N_s \times N_t}$ ($N_s = N_u - \sum_i I'(\mathbf{H}_i)$) can be optimized by the OT problem (5). To solve the problem (5), simplex methods can be used, e.g., the network simplex algorithm with a complexity of $\mathcal{O}((N_s + N_t)^3 \log(N_s + N_t)^2)$ [39], [47]. Moreover, low-complexity algorithms can be adopted to approximately solve (5), e.g., the Sinkhorn algorithm [37], [38], [45] with a complexity of $\mathcal{O}(I_{\text{Iter}} N_s N_t)$, where I_{Iter} is the number of Sinkhorn iterations.

Once the optimal joint probability matrix Γ^* is obtained, the transformed position for each identified NLoS user can be written as [37]

$$\tilde{\mathbf{P}}_{\text{NLoS}} = \text{diag}(\Gamma^* \cdot \mathbf{1}_{N_t})^{-1} \cdot \Gamma^* \cdot \bar{\mathbf{P}}, \quad (30)$$

where $\bar{\mathbf{P}} \in \mathbb{R}^{N_t \times 3}$ is the collection of all $\{\tilde{\mathbf{p}}_i\}_{i=1,2,\dots,N_t}$; $\tilde{\mathbf{P}}_{\text{NLoS}} \in \mathbb{R}^{N_s \times 3}$ with $[\tilde{\mathbf{P}}_{\text{NLoS}}]_{i,:} = \mathbf{T}^*(\hat{\mathbf{p}}_i^{\text{mb}})$ being the mapped position⁶. Then, combining the identified LoS and NLoS user positions, the self-generated labels $\{\tilde{\mathbf{p}}_i\}_{i=1,2,\dots,N_u}$ can be expressed as

$$\tilde{\mathbf{p}}_i = \begin{cases} \hat{\mathbf{p}}_i^{\text{mb}}, & \text{if } I'(\mathbf{H}_i) = 1; \\ \mathbf{T}^*(\hat{\mathbf{p}}_i^{\text{mb}}), & \text{if } I'(\mathbf{H}_i) = 0. \end{cases} \quad (31)$$

B. NN-model Training

From the CSI dataset $\{\mathbf{H}_i\}_{i=1,2,\dots,N_u}$, where the ground-truth positions $\{\mathbf{p}_i\}$ are not available in accordance with unsupervised learning, a transformed dataset $\mathcal{S}'' = \{\mathbf{s}_i, \tilde{\mathbf{p}}_i\}_{i=1,2,\dots,N_u}$ can be obtained by applying $\mathbf{s}_i = f_{\text{extr}}(\mathbf{H}_i)$ and the training label self-generation (31). Then, the NN model can be trained by a fingerprinting loss and the optional triplet loss (if timestamps are available), which can be written as

$$\mathcal{L} = \frac{1}{N_u} \sum_{\mathbf{s}_i, \tilde{\mathbf{p}}_i \in \mathcal{S}''} \|\mathbf{s}_i - \tilde{\mathbf{p}}_i\|_2^2 + \omega_{\text{Tri}} \cdot \mathcal{L}_{\text{Tri}}, \quad (32)$$

where $\omega_{\text{Tri}} \geq 0$ is a non-negative coefficient ($\omega_{\text{Tri}} = 0$ and \mathcal{L}_{Tri} is not included if timestamps are not available). Note that the training of the NN model in UNILoc does not involve OT, and thus with the self-generated labels $\{\tilde{\mathbf{p}}_i\}$, the parameters Θ can be updated by backpropagation by only tracing back through the NN model. For an L_{MLP} -layer MLP, the training complexity of UNILoc is $\mathcal{O}(N_u \sum_{l=1}^{L_{\text{MLP}}} n_{l-1} n_l)$ per epoch, which is much lower than that of UNILocPro, i.e., $\mathcal{O}(N_u \sum_{l=1}^{L_{\text{MLP}}} n_{l-1} n_l + I_{\text{Iter}} N_u N_t)$ per epoch, especially for large-scale datasets.

Remark: It is noted that UNILoc can be regarded as a specific implementation of UNILocPro by setting $\kappa \rightarrow \infty$ in (18), $\alpha_{i,j} = 1$ in (20), and detaching the OT-based loss \mathcal{L}_{OT} from the iterative training process. Actually, the dissimilarity metric $\{d_{i,j}^{\text{Fusi}}\}$ would be the pairwise distance of $\{\hat{\mathbf{p}}_i^{\text{mb}}\}_{i=1,2,\dots,N_u}$ when $\alpha_{i,j} = 1$ and $\kappa \rightarrow \infty$ such that the pairwise distance loss \mathcal{L}_{PWD} and the LoS-based loss \mathcal{L}_{LOS} would generate a channel chart that is exactly the model-based estimates $\{\hat{\mathbf{p}}_i^{\text{mb}}\}_{i=1,2,\dots,N_u}$. Then, applying the OT-based loss \mathcal{L}_{OT} once would generate the self-generated labels $\{\tilde{\mathbf{p}}_i\}$, which are used as training labels for the NN model in UNILoc.

VII. NUMERICAL EXPERIMENTS

A. System Setting

In this section, numerical experiments in a street canyon scenario, as shown in Fig. 1, are carried out. The carrier frequency of the system is $f_c = 10$ GHz, and 50 MHz bandwidth is used with a subcarrier spacing of 120 kHz. Being equipped with a ULA ($M = 256$ antennas and the inter-antenna distance is set as $d = \lambda/2$), the BS is placed at $\mathbf{p}_{\text{BS}} = [0, -9, 57]^T$, and the height of each user position is set as 1.5 m, i.e., $\mathbf{p}_i = [x_i, y_i, 1.5]^T$. User positions in both training and testing datasets are generated randomly according to a uniform distribution in the first quadrant of the map. For each user position, the CSI \mathbf{H}_i is generated realistically by Sionna RT [27], where ray-tracing techniques are used to generate the propagation paths, based on which the channel \mathbf{H}_i is computed. Around 1800 user positions, consisting of 550 LoS and 1250 NLoS, are generated independently for both training and testing datasets (as unsupervised learning is considered in this paper, the ground-truth positions $\{\mathbf{p}_i\}$ in the training dataset are only used for validation). When using OT in \mathcal{L}_{OT} (26) and in label self-generation (30), the target domain $\mathcal{X}_t = \{\bar{\mathbf{p}}_i\}_{i=1,2,\dots,N_t}$ is generated by selecting N_t grid points in the NLoS region, i.e., $\bar{\mathbf{p}}_i \in \mathcal{G}_{\text{NLoS}} \subseteq \mathcal{R}_{\text{NLoS}}$, where $\mathcal{G}_{\text{NLoS}}$ contains all grid points with a spacing distance of $\Delta_d = 0.5$ m in $\mathcal{R}_{\text{NLoS}}$.

For the training dataset $\{\mathbf{H}_i, \mathbf{p}_i\}$, the timestamps $\{t_i\}$ are generated as $t_0 = 0$ and $t_i = t_{i-1} + \frac{\|\mathbf{p}_i - \mathbf{p}_{i-1}\|_2}{v_i}$, $i > 1$ along the shortest trajectory; and v_i is the velocity in the i -th segment of the trajectory. With consideration of velocity variation, we set v_k as a truncated Gaussian random variable, i.e., $v_k = \max(0, v'_k)$, where $v'_k \sim \mathcal{N}(\mu, \sigma_v^2)$ with μ being the mean velocity and σ_v being the standard deviation. Without other specifications, we set $\mu = 10$ m/s and $\sigma_v = 0$ m/s. When generating the triplet set \mathcal{T} , we set $T_{\text{L}} = 10/\mu$ and $T_{\text{U}} = 50/\mu$ in (23). Note that the timestamps $\{t_i\}$ are only generated for the training dataset, and not needed for the testing dataset.

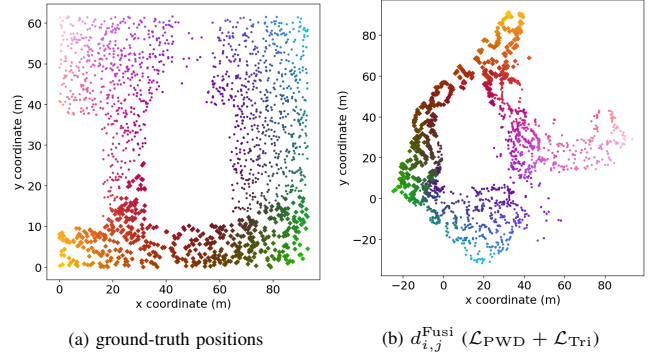


Fig. 6: Channel chart generated by $\{d_{i,j}^{\text{Fusi}}\}$ with timestamps (training dataset; every user is associated with a unique color; dot marks represent NLoS user positions and diamond marks represent LoS user positions).

TABLE I: The CC performance for different dissimilarity metrics.

Dissimilarity metric	$\mathcal{CT} \uparrow$	$\mathcal{TW} \uparrow$	$\mathcal{KS} \downarrow$
without timestamps			
$d_{i,j}^{\text{G-CIRA}} (\mathcal{L}_{\text{PWD}})$	0.824	0.827	0.712
$d_{i,j}^{\text{G-Fro}} (\mathcal{L}_{\text{PWD}})$	0.770	0.773	0.540
$d_{i,j}^{\text{G-Corr}} (\mathcal{L}_{\text{PWD}})$	0.852	0.816	0.478
$d_{i,j}^{\text{G-ADP}} (\mathcal{L}_{\text{PWD}})$	0.836	0.768	0.432
$d_{i,j}^{\text{G-GOSPA}} (\mathcal{L}_{\text{PWD}})$	0.950	0.960	0.273
$d_{i,j}^{\text{Wass}} (\mathcal{L}_{\text{PWD}})$	0.971	0.971	0.262
$d_{i,j}^{\text{Fusi}} (\mathcal{L}_{\text{PWD}})$	0.980	0.980	0.206
with timestamps			
$d_{i,j}^{\text{time}} (\mathcal{L}_{\text{PWD}})$	0.763	0.709	0.593
\mathcal{L}_{Tri}	0.907	0.749	0.536
$d_{i,j}^{\text{G-Fusi-ADP}} (\mathcal{L}_{\text{PWD}})$	0.915	0.924	0.306
$d_{i,j}^{\text{G-Fro}} (\mathcal{L}_{\text{PWD}} + \mathcal{L}_{\text{Tri}})$	0.928	0.831	0.467
$d_{i,j}^{\text{G-Corr}} (\mathcal{L}_{\text{PWD}} + \mathcal{L}_{\text{Tri}})$	0.933	0.866	0.461
$d_{i,j}^{\text{G-ADP}} (\mathcal{L}_{\text{PWD}} + \mathcal{L}_{\text{Tri}})$	0.962	0.913	0.314
$d_{i,j}^{\text{G-GOSPA}} (\mathcal{L}_{\text{PWD}} + \mathcal{L}_{\text{Tri}})$	0.986	0.983	0.241
$d_{i,j}^{\text{Wass}} (\mathcal{L}_{\text{PWD}} + \mathcal{L}_{\text{Tri}})$	0.981	0.974	0.226
$d_{i,j}^{\text{Fusi}} (\mathcal{L}_{\text{PWD}} + \mathcal{L}_{\text{Tri}})$	0.988	0.986	0.180

For the hyper-parameters involved in this paper, we set the regularization parameter $\varepsilon = 2/3$ in (27) when conducting the Sinkhorn iteration; the trust region distance $\zeta = 20$ is adopted for computing the GOSPA-based dissimilarity (15); when fusing the GOSPA-based and Wasserstein-based metrics, we use $\vartheta = 0.03$ and $d_{\text{thre}} = 10$ in (21); when computing the triplet loss (13), $\gamma = 0.1$ is used. As all of the loss terms in (9) (resp. (32)) have similar magnitudes, we set $\omega_{\text{C-CC}} = 1$, $\omega_{\text{LoS}} = 1$, $\omega_{\text{OT}} = 1$, $\omega_{\text{PWD}} = 1$, and $\omega_{\text{Tri}} = 1$ (resp. $\omega_{\text{Tri}} = 1$) when timestamps are available without other specifications ($\omega_{\text{Tri}} = 0$ if timestamps are not available).

As for the NN model, following the same NN architecture and hyper-parameters as in [15], [17], an MLP is adopted for $f_{\Theta}(\cdot)$, which consists of 5 hidden layers (each with 1024, 512, 256, 128, 64 neurons, respectively, ReLU activation, and batch normalization) and an output layer (with 2 neurons and linear activation). Moreover, Adam optimizer with a decayed learning rate is employed for training. All the NN models are implemented in TensorFlow and the training is performed on a machine with a NVIDIA Tesla T4 GPU (16 GB RAM).

B. CC Results

We would like to evaluate the CC performance of different dissimilarity metrics, including our proposed GOSPA-based and Wasserstein-based metrics, as well as some dissimilarity

TABLE II: Positioning error for different localization methods (testing dataset).

	MAE (m)			RMSE (m)			95th percentile error (m)		
	LoS	NLoS	all	LoS	NLoS	all	LoS	NLoS	all
Unsupervised Methods without Timestamps									
model-based method	0.34	13.79	9.81	0.61	17.78	14.92	1.11	32.41	31.21
UNILocPro ($p_I = 1$)	0.34	7.21	5.18	0.61	9.48	7.96	1.11	18.03	15.99
conservative UNILocPro	0.52	7.83	5.67	1.60	10.09	8.51	1.94	20.78	18.77
UNILoc ($p_I = 1$)	0.34	7.67	5.50	0.61	9.87	8.29	1.11	18.47	17.05
conservative UNILoc	0.51	8.49	6.13	1.58	11.05	9.31	1.94	22.32	19.41
Unsupervised Methods with Timestamps									
UNILocPro ($p_I = 1$)	0.34	5.77	4.17	0.61	7.42	6.24	1.11	14.24	12.44
conservative UNILocPro	0.49	6.87	4.98	1.39	8.91	7.52	1.94	18.94	16.46
UNILoc ($p_I = 1$)	0.34	6.37	4.59	0.61	7.98	6.71	1.11	14.39	13.36
conservative UNILoc	0.42	6.97	5.03	1.02	8.70	7.32	1.64	16.26	14.71
Semi-supervised Methods with Timestamps									
CC-based method ($d_{i,j}^{\text{G-Fusi-ADP}}$)	12.68	14.16	13.71	14.37	16.02	15.54	25.67	26.29	25.91
CC-based method with OT ($d_{i,j}^{\text{G-Fusi-ADP}}$)	15.09	17.02	16.45	18.87	19.97	19.65	37.15	33.99	34.94
Supervised Methods									
fingerprinting ($\Delta_s = 2$ m)	4.69	6.06	5.65	6.02	7.87	7.36	11.66	14.81	13.71
fingerprinting ($\Delta_s = 1$ m)	3.89	5.43	4.98	4.84	7.42	6.75	8.56	14.78	12.81
fingerprinting ($\Delta_s = 0.5$ m)	3.95	4.48	4.46	4.85	6.61	6.13	9.16	12.07	11.02

metrics used in the literature: 1) a CSI Frobenius norm-based metric $d_{i,j}^{\text{Fro}}$ [21, Eq. (1)]; 2) a CSI correlation-based metric $d_{i,j}^{\text{Corr}}$ [14, Eq. (2)]; 3) a metric based on channel impulse response amplitude $d_{i,j}^{\text{CIRA}}$ [22, Eq. (15)]; 4) a dissimilarity metric based on channel angle-delay profile $d_{i,j}^{\text{ADP}}$ [17, Eq. (6)]; 5) the time difference $d_{i,j}^{\text{time}}$ in (22); 6) a fusion of $d_{i,j}^{\text{time}}$ and $d_{i,j}^{\text{ADP}}$, as denoted by $d_{i,j}^{\text{Fusi-ADP}}$ [17, Eq. (15)]; and 7) the geodesic variants of these metrics (denoted with the prefix “G-”), including $d_{i,j}^{\text{G-Fro}}$, $d_{i,j}^{\text{G-Corr}}$, $d_{i,j}^{\text{G-CIRA}}$, $d_{i,j}^{\text{G-ADP}}$, and $d_{i,j}^{\text{G-Fusi-ADP}}$. Without timestamps, only the pairwise distance loss \mathcal{L}_{PWD} (11) based on these dissimilarity metrics is used to train the NN model $f_{\Theta}(\cdot)$, i.e., $\mathcal{L} = \mathcal{L}_{\text{PWD}}$. When timestamps are available, the triplet loss \mathcal{L}_{Tri} (13) constructed by $\{t_i\}$ can be integrated with the pairwise distance loss \mathcal{L}_{PWD} for enhancement, i.e., $\mathcal{L} = \mathcal{L}_{\text{PWD}} + \mathcal{L}_{\text{Tri}}$.

In order to quantify the CC performance, we use the continuity ($0 \leq \mathcal{CT} \leq 1$), the trustworthiness ($0 \leq \mathcal{TW} \leq 1$), and the Kruskal stress ($0 \leq \mathcal{KS} \leq 1$) to evaluate different dissimilarity metrics [14], [15], [17], [41]. The CC performance of different dissimilarity metrics is summarized in Table I. It is observed that the proposed GOSPA-based and Wasserstein-based metrics significantly outperform the state-of-the-art dissimilarity metrics, and their fusion achieves the best performance. It is also seen that the timestamps cannot generate a good channel chart directly, e.g., by using $d_{i,j}^{\text{time}}$ or the triplet loss \mathcal{L}_{Tri} alone, but it can improve CC performance significantly for existing metrics through adding the triplet loss \mathcal{L}_{Tri} . Moreover, as shown in Fig. 6, the proposed metrics not only achieve remarkable CC performance, but also preserve the overall global spatial structure (up to a rotation and translation ambiguity) as the basic shape of the channel chart closely resembles the ground-truth positions. This phenomenon would have a positive impact on localization, as will be shown next.

C. Localization Results

For evaluation and analysis, mean absolute error (MAE), root mean square error (RMSE), and 95th percentile error are adopted as metrics for localization, i.e., $\text{MAE} = \frac{1}{N_u} \sum_i \|\hat{\mathbf{p}}_i - \mathbf{p}_i\|_2$, $\text{RMSE} = (\frac{1}{N_u} \sum_i \|\hat{\mathbf{p}}_i - \mathbf{p}_i\|_2^2)^{\frac{1}{2}}$, and

$E_{95\%} = \text{prc}(\{\|\hat{\mathbf{p}}_i - \mathbf{p}_i\|_2\}, 95)$, where $\text{prc}(\cdot, \alpha_p)$ is the α_p -th percentile of the set. For comparison, in addition to UNILocPro and UNILoc, model-based, fingerprinting, and CC-based localization methods are considered as benchmarks:

- **Model-based method**: position estimates are obtained based on the OMP algorithm and geometric relationships, i.e., $\hat{\mathbf{p}}_i^{\text{mb}} = f_{\text{pe}}[f_{\text{ce}}(\mathbf{H}_i)]$, $\forall i$;
- **Fingerprinting**: position estimates are obtained from NN, i.e., $\hat{\mathbf{p}}_i^{\text{nb}} = f_{\Theta}[\mathbf{f}_{\text{extr}}(\mathbf{H}_i)]$, where $f_{\Theta}(\cdot)$ is trained by assuming ground-truth labels, i.e., $\tilde{\mathbf{p}}_i = \mathbf{p}_i$, $\forall i$. It is a fully-supervised approach;
- **CC-based method ($d_{i,j}^{\text{G-Fusi-ADP}}$)** [17]: position estimates are obtained as $\hat{\mathbf{p}}_i = \mathbf{T}(f_{\Theta}[\mathbf{f}_{\text{extr}}(\mathbf{H}_i)])$, where the NN model $f_{\Theta}(\cdot)$ is trained based on the pairwise distance loss \mathcal{L}_{PWD} (11) with $d_{i,j} = d_{i,j}^{\text{G-Fusi-ADP}}$, and $\mathbf{T}(\mathbf{p}) = \mathbf{A}^* \cdot \mathbf{p} + \mathbf{b}^*$ is the optimal affine transformation that solves the following least squares (LS) problem: $\mathbf{A}^*, \mathbf{b}^* = \arg \min_{\mathbf{A}, \mathbf{b}} \sum_i \|\mathbf{A} \cdot f_{\Theta}[\mathbf{f}_{\text{extr}}(\mathbf{H}_i)] + \mathbf{b} - \mathbf{p}_i\|_2^2$, where $\mathbf{A} \in \mathbb{R}^{3 \times 3}$ is a rotation and scaling matrix, and $\mathbf{b} \in \mathbb{R}^{3 \times 1}$ is a translation vector. It is a semi-supervised approach;
- **CC-based method with OT ($d_{i,j}^{\text{G-Fusi-ADP}}$)**: position estimates are obtained as $\hat{\mathbf{p}}_i = \mathbf{T}_{\text{OT}}(\mathbf{T}(f_{\Theta}[\mathbf{f}_{\text{extr}}(\mathbf{H}_i)]))$, where the NN model $f_{\Theta}(\cdot)$ and the affine transformation $\mathbf{T}(\cdot)$ are the same as the CC-based method ($d_{i,j}^{\text{G-Fusi-ADP}}$); and $\mathbf{T}_{\text{OT}}(\cdot)$ is a transformation that maps $\{\mathbf{T}(f_{\Theta}[\mathbf{f}_{\text{extr}}(\mathbf{H}_i)])\}$ to grid positions in \mathcal{R} with a spacing distance of Δ_d via OT. It is a semi-supervised approach.

In this section, we also implement the conservative variant of UNILoc and UNILocPro, where the conservative LoS/NLoS identification (8) is adopted instead of (7). For a fair comparison, as fingerprinting requires extensive CSI measurement and collection, the dataset often contains limited data samples. For fingerprinting, grid positions on the map with corresponding CSI are used for training. Specifically, around 1800 user positions are selected from all grid points on the map, denoted by \mathcal{G} , with a spacing distance of Δ_s , i.e., $\mathbf{p}_i \in \mathcal{G} \subseteq \mathcal{R}$, $\forall i$. Note that if \mathcal{G} has fewer than 1800 positions, all grid positions in \mathcal{G}

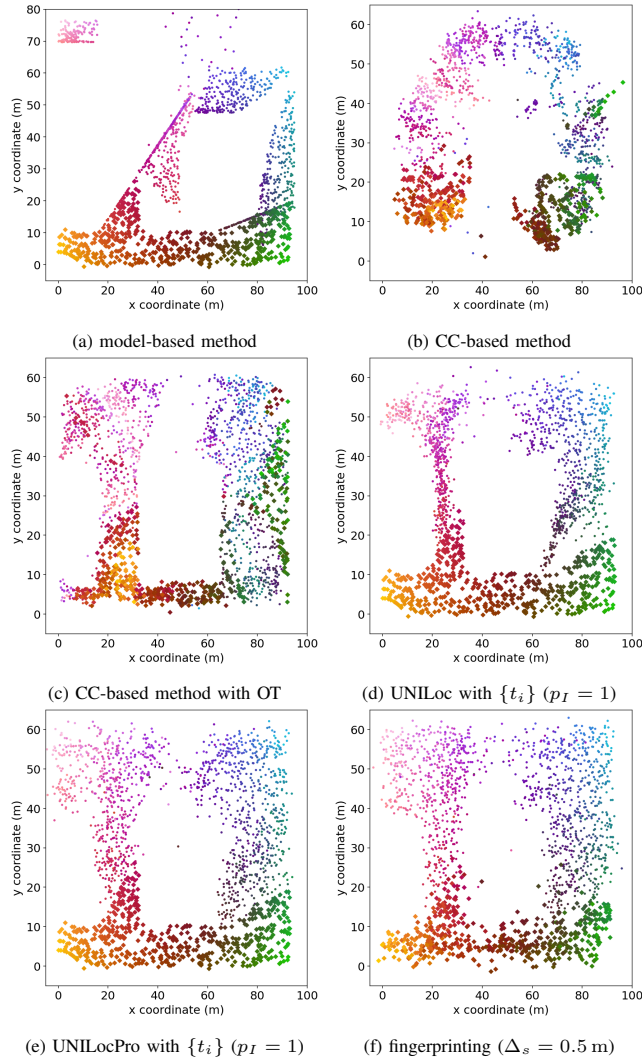


Fig. 7: Position estimates for different localization methods (testing dataset; every user is associated with a unique color; dot marks represent NLoS user positions and diamond marks represent LoS user positions).

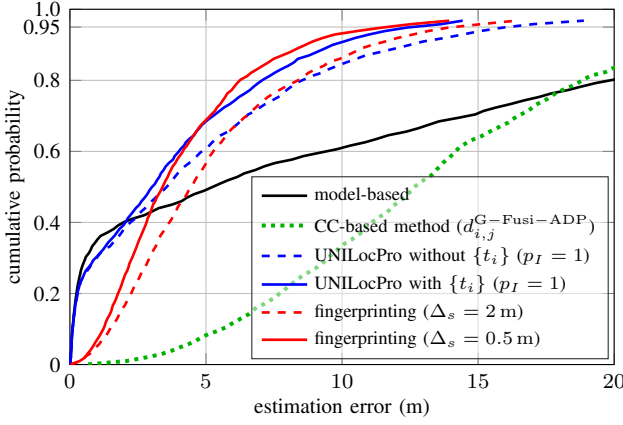


Fig. 8: The cumulative distribution function (CDF) w.r.t. the positioning error for different methods (testing dataset).

are selected. While testing, user positions are placed randomly, which is the same as in the other methods considered.

1) Positioning Accuracy

Fig. 7 shows the position estimates for different localization methods; for a quantitative evaluation, the CDF of estimation

errors and performance metrics are also shown in Fig. 8 and Table II, respectively. It is observed that the model-based method achieves high positioning accuracy for LoS users ($MAE = 0.34\text{ m}$), while the estimates for NLoS users are significantly distorted. The fingerprinting with a small Δ_s has the lowest estimation error for NLoS user positions (also preserves the global shape of NLoS users), while the estimates of LoS users are not as precise as those produced by the model-based method. Being an integrated strategy, UNILoc and UNILocPro (as well as the conservative variant) can not only attain precise estimations for LoS users but also preserve the global position of the NLoS users, demonstrating the effectiveness of the integration model-based geometry and CC, the new dissimilarity metrics, and the OT-based loss. This indicates that the model-based methods could provide valuable information for unsupervised learning approaches to improve estimation accuracy. Moreover, UNILocPro is able to provide better localization compared with UNILoc, as UNILocPro incorporates OT loss during training rather than a single-shot OT application before training, which offers a global geometry that is close to the ground-truth positions.

It can also be seen that although the local geometry, i.e., the neighboring relationship between user positions, is preserved in general, the CC-based method ($d_{i,j}^{G-Fusi-ADP}$) cannot capture the global geometry due to the lack of physical distance information in the dissimilarity metric, resulting in large position estimation errors. Note that adding the OT directly to the CC-based method ($d_{i,j}^{G-Fusi-ADP}$) could not improve the performance (on the contrary, it would deteriorate positioning accuracy), which highlights that OT can only improve localization performance when the generated channel chart is sufficiently good, i.e., the local geometry is preserved and the global geometry is not very far from the ground-truth positions. This is because the OT, which performs a transformation based solely on transportation cost minimization (this process is purely metric-related and lacks higher-level geometric constraints), can only refine a localization estimate but cannot directly recover the underlying global geometry autonomously. In other words, the OT cannot correct large errors in the position estimates.

It is intuitive that introducing timestamps would further improve the performance of UNILoc and UNILocPro. Notably, UNILocPro with timestamps ($MAE = 4.17\text{ m}$ and $RMSE = 6.24\text{ m}$) achieves performance very close to that of fully-supervised fingerprinting with $\Delta_s = 0.5\text{ m}$ ($MAE = 4.46\text{ m}$ and $RMSE = 6.13\text{ m}$). It is also noted that without external LoS/NLoS identification, the conservative variant of UNILocPro can still achieve satisfactory performance (close to the fully-supervised fingerprinting with $\Delta_s = 2\text{ m}$). This indicates that the proposed unified localization frameworks do not rely on external LoS/NLoS identification and are also robust to the identification accuracy, should one be available.

2) Discussion on p_I

In order to explore the impact of the LoS/NLoS identification accuracy, Fig. 9 shows the MAE of UNILocPro with timestamps for different p_I (a similar figure can be obtained for UNILocPro without timestamps). It is clear

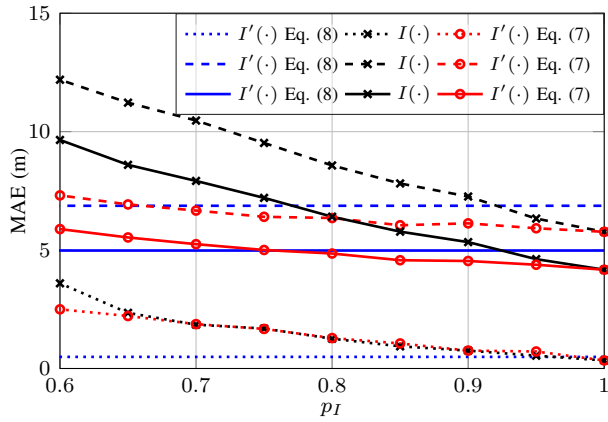


Fig. 9: The MAE of UNILocPro with timestamps for different p_I (testing dataset; the dotted lines represent LoS user positions; the dashed lines represent NLoS user positions; the solid lines represent all user positions).

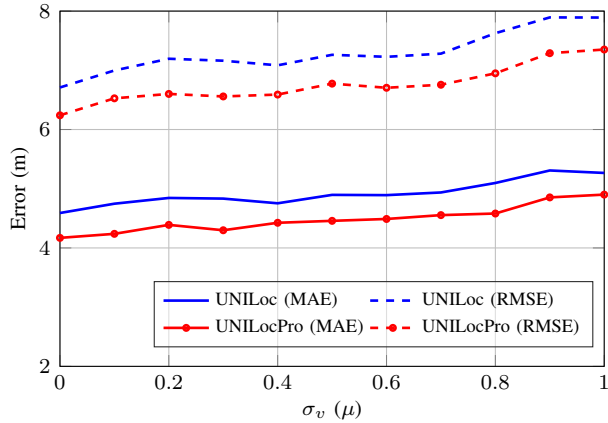


Fig. 10: The testing error of UNILoc and UNILocPro with timestamps for different σ_v used in training.

(also intuitive) that the performance of UNILocPro (the same for UNILoc) depends on the identification accuracy p_I , and its estimation error would increase with the reduction of p_I ; however, using the model-based estimations to improve the LoS/NLoS identification (7) can significantly reduce the position estimation error compared with the case relying on the identification mechanism $I(\cdot)$ only. This verifies that the model-based methods can provide information to improve the LoS/NLoS identification or even replace the identification mechanism $I(\cdot)$ (as the conservative UNILocPro performs quite well), which is one of the advantages of the proposed unified localization frameworks. It also can be observed that for a reasonable $p_I \in [0.93, 1]$ (from the existing identification methods in the literature), UNILocPro (UNILoc) performs better than its conservative variant overall. There is a critical $p_I \approx 0.76$ (resp. $p_I \approx 0.82$) when timestamps are (resp. are not) available, corresponding to the intersection point of the overall MAE, below which the conservative method is a better choice. This implies that a dynamic switch between UNILocPro (UNILoc) and its conservative variant based on p_I can be adopted.

3) Discussion on Velocity Variation

Then, we investigate the impact of velocity variation on the CC and localization performance. The channel chart generated by the triplet loss \mathcal{L}_{Tri} for different $\sigma_v = 0.5\mu$ (resp. $\sigma_v =$

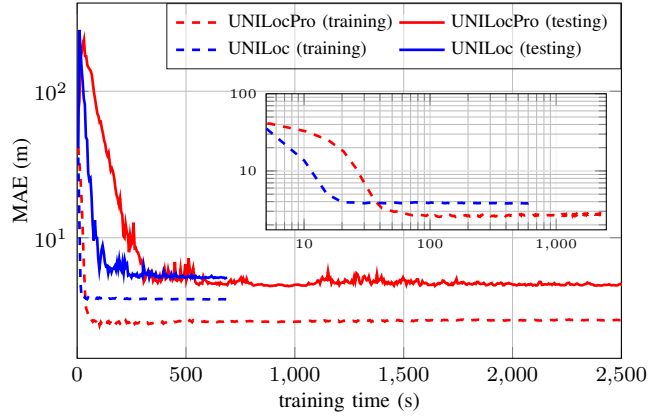


Fig. 11: The MAE of UNILoc and UNILocPro with timestamps during training.

μ) achieves $\mathcal{CT} = 0.856$, $\mathcal{TW} = 0.720$, and $\mathcal{KS} = 0.544$ (resp. $\mathcal{CT} = 0.733$, $\mathcal{TW} = 0.664$, and $\mathcal{KS} = 0.594$), which shows that the channel chart is distorted significantly when σ_v increases compared with the case with $\sigma_v = 0$. As shown in Fig. 10, where the MAE and RMSE are plotted w.r.t. the velocity variation from $\sigma_v = 0$ to $\sigma_v = \mu$, it is intuitive that the increase of σ_v would deteriorate the localization performance; however, UNILoc and UNILocPro are quite robust to the velocity variation, and the MAE and RMSE of UNILocPro are 4.90 m and 7.35 m when $\sigma_v = \mu$, which is still better than the case without timestamps, and only within around 1 m larger than that when $\sigma_v = 0$ (MAE = 4.17 m and RMSE = 6.24 m). This indicates that the proposed unified frameworks, by integrating the model-based pairwise distance loss \mathcal{L}_{PWD} and the OT-based loss \mathcal{L}_{OT} , can effectively mitigate the impact of velocity variation on localization performance. In other words, the timestamps, even if not accurate, can still help to improve localization in our proposed unified frameworks by providing additional information about the user positions.

4) Discussion on Training Complexity

Finally, we would compare the training complexity of UNILoc and UNILocPro by examining the MAE during training, as shown in Fig. 11. Without computation and back-propagation of the iterative Sinkhorn algorithm, the training of UNILoc is much faster than that of UNILocPro (around 4 to 5 times faster in our experiments), which implies that the training complexity of UNILoc is much lower than that of UNILocPro. It also takes a much longer time for UNILocPro before its testing performance becomes stable. Note that with reduced training complexity, UNILoc only leads to slightly degraded performance (within 0.5 m in our experiments) compared to UNILocPro (for example, when timestamps are available, the MAE and RMSE of UNILocPro are 4.17 m and 6.24 m, while the MAE and RMSE of UNILoc are 4.59 m and 6.71 m). This suggests that the simplified UNILoc is more efficient and suitable for large-scale datasets, while UNILocPro can be utilized when training complexity is not a concern.

VIII. CONCLUSION AND FUTURE WORK

In this paper, we propose unified localization frameworks by combining model-based geometry and CC for mixed LoS/NLoS scenarios. For achieving unsupervised CC, we first design two new dissimilarity metrics (and their fusion), which are shown not only to achieve good CC performance but also to

preserve the basic global geometry, and then the CC model of UNILocPro is trained by integrating multiple losses. Moreover, a low-complexity variant, i.e., UNILoc, is also proposed by simplifying the OT-based loss. Neither of the proposed methods requires ground-truth labels, and they can also work without timestamps and the external LoS/NLoS identification. Ray-tracing simulations are carried out to show that the proposed frameworks significantly outperform the model-based and the CC-based methods in terms of both CC and global localization performance. Notably, UNILocPro with timestamps can achieve close positioning performance (almost the same overall in our experiments) compared with the fully-supervised fingerprinting. It is also shown that the proposed frameworks are robust to the LoS/NLoS identification error and velocity variation, and UNILoc can reduce the training complexity significantly with marginal performance degradation compared with UNILocPro. The extension of this work includes rigorous validation through real-world testbed experiments and an in-depth analysis of map mismatch robustness.

REFERENCES

- [1] Y. Zhang, G. Pan, M. F. Keskin, O. Kaltiokallio, M. Valkama, and H. Wymeersch, “UNILoc: Unified localization combining model-based geometry and unsupervised learning,” in *Proc. IEEE Globecom*, Dec. 2025, pp. 1–6.
- [2] K. Witrisal *et al.*, “High-accuracy localization for assisted living: 5G systems will turn multipath channels from foe to friend,” *IEEE Signal Process. Mag.*, vol. 33, no. 2, pp. 59–70, Mar. 2016.
- [3] H. Chen *et al.*, “A tutorial on terahertz-band localization for 6G communication systems,” *IEEE Commun. Surveys Tuts.*, vol. 24, no. 3, pp. 1780–1815, May 2022.
- [4] Z. Wang *et al.*, “Near-field localization and sensing with large-aperture arrays: From signal modeling to processing,” *IEEE Signal Process. Mag.*, vol. 42, no. 1, pp. 74–87, Jan 2025.
- [5] R. Zekavat and R. M. Buehrer, *An Introduction to NLOS Identification and Localization*, 2012, pp. 523–555.
- [6] R. Mendarzik *et al.*, “Harnessing NLOS components for position and orientation estimation in 5G millimeter wave MIMO,” *IEEE Trans. Wireless Commun.*, vol. 18, no. 1, pp. 93–107, Jan. 2019.
- [7] F. Zafari, A. Gkelias, and K. K. Leung, “A survey of indoor localization systems and technologies,” *IEEE Commun. Surveys Tuts.*, vol. 21, no. 3, pp. 2568–2599, Apr. 2019.
- [8] O. Kaltiokallio *et al.*, “Robust snapshot radio SLAM,” *IEEE Trans. Veh. Technol.*, vol. 74, no. 5, pp. 8460–8465, May 2025.
- [9] X. Sun *et al.*, “Fingerprint-based localization for massive MIMO-OFDM system with deep convolutional neural networks,” *IEEE Trans. Veh. Technol.*, vol. 68, no. 11, pp. 10846–10857, Nov. 2019.
- [10] G. Pan, Y. Gao, Y. Gao, Z. Zhong, X. Yang, X. Guo, and S. Xu, “AI-driven wireless positioning: Fundamentals, standards, state-of-the-art, and challenges,” *arXiv preprint arXiv:2501.14970*, 2025.
- [11] C. Wu *et al.*, “Learning to localize: A 3D CNN approach to user positioning in massive MIMO-OFDM systems,” *IEEE Trans. Wireless Commun.*, vol. 20, no. 7, pp. 4556–4570, Jul. 2021.
- [12] G. Pan *et al.*, “Large wireless localization model (LWLM): A foundation model for positioning in 6G networks,” *arXiv preprint arXiv:2505.10134*, 2025.
- [13] J. A. Tropp and A. C. Gilbert, “Signal recovery from random measurements via orthogonal matching pursuit,” *IEEE Trans. Inf. Theory*, vol. 53, no. 12, pp. 4655–4666, Dec. 2007.
- [14] C. Studer *et al.*, “Channel charting: Locating users within the radio environment using channel state information,” *IEEE Access*, vol. 6, pp. 47682–47698, Aug. 2018.
- [15] P. Ferrand, A. Decurninge, L. G. Ordoñez, and M. Guillaud, “Triplet-based wireless channel charting: Architecture and experiments,” *IEEE J. Sel. Areas Commun.*, vol. 39, no. 8, pp. 2361–2373, Aug. 2021.
- [16] F. Euchner, P. Stephan, and S. t. Brink, “Augmenting channel charting with classical wireless source localization techniques,” in *Proc. IEEE Asilomar*, Oct. 2023, pp. 1641–1647.
- [17] P. Stephan, F. Euchner, and S. t. Brink, “Angle-delay profile-based and timestamp-aided dissimilarity metrics for channel charting,” *IEEE Trans. Commun.*, vol. 72, no. 9, pp. 5611–5625, Sept. 2024.
- [18] O. Esrafilian *et al.*, “Global scale self-supervised channel charting with sensor fusion,” in *Proc. IEEE Globecom Workshops*, Dec. 2024, pp. 1–6.
- [19] L. Cazzella *et al.*, “Chartwin: a case study on channel charting-aided localization in dynamic digital network twins,” *arXiv preprint arXiv:2508.09055*, 2025.
- [20] M. Maleki *et al.*, “Channel charting in smart radio environments,” *arXiv preprint arXiv:2508.07305*, 2025.
- [21] J. Pihlajasalo, M. Koivisto, J. Talvitie, S. Ali-Löytty, and M. Valkama, “Absolute positioning with unsupervised multipoint channel charting for 5G networks,” in *Proc. IEEE VTC-Fall*, Nov. 2020, pp. 1–5.
- [22] M. Stahlke *et al.*, “Indoor localization with robust global channel charting: A time-distance-based approach,” *IEEE Trans. Mach. Learn. Commun. Netw.*, vol. 1, pp. 3–17, Mar. 2023.
- [23] L. Zhao *et al.*, “A signature based approach towards global channel charting with ultra low complexity,” in *Proc. IEEE ICC Workshops*, Jun. 2024, pp. 667–672.
- [24] F. Euchner, P. Stephan, and S. t. Brink, “Leveraging the doppler effect for channel charting,” in *Proc. IEEE SPAWC*, Sept. 2024, pp. 731–735.
- [25] F. G. Zanjani *et al.*, “Modality-agnostic topology aware localization,” in *Proc. NeurIPS*, Dec. 2021.
- [26] M. Stahlke *et al.*, “Velocity-based channel charting with spatial distribution map matching,” *IEEE J. Indoor Seamless Position. Navig.*, vol. 2, pp. 230–239, Jul. 2024.
- [27] J. Hoydis *et al.*, “Sionna,” 2022, <https://nvlabs.github.io/sionna/>.
- [28] M. Ahadi *et al.*, “TDoA-based self-supervised channel charting with NLoS mitigation,” *arXiv preprint arXiv:2510.08001*, 2025.
- [29] V. Koivunen *et al.*, “Multicarrier ISAC: Advances in waveform design, signal processing, and learning under nonidealities,” *IEEE Signal Process. Mag.*, vol. 41, no. 5, pp. 17–30, Sept. 2024.
- [30] J. M. Mateos-Ramos *et al.*, “Model-based end-to-end learning for multi-target integrated sensing and communication under hardware impairments,” *IEEE Trans. Wireless Commun.*, vol. 24, no. 3, pp. 2574–2589, Mar. 2025.
- [31] M. F. Keskin *et al.*, “Fundamental trade-offs in monostatic ISAC: A holistic investigation towards 6G,” *IEEE Trans. Wireless Commun.*, vol. 24, no. 9, pp. 7856–7873, Sept. 2025.
- [32] E. Björnson, J. Hoydis, and L. Sanguinetti, *Massive MIMO Networks: Spectral, Energy, and Hardware Efficiency*. Found. Trends Signal Process., 2017, vol. 11, no. 3–4.
- [33] J. Pinto, Y. Xia, L. Svensson, and H. Wymeersch, “An uncertainty-aware performance measure for multi-object tracking,” *IEEE Signal Process. Lett.*, vol. 28, pp. 1689–1693, Aug. 2021.
- [34] Y. Wang, Y. Sun, J. Wang, and Y. Shen, “Dynamic spectrum tracking of multiple targets with time-sparse frequency-hopping signals,” *IEEE Signal Process. Lett.*, vol. 31, pp. 1675–1679, Jun. 2024.
- [35] A. S. Rahmathullah *et al.*, “Generalized optimal sub-pattern assignment metric,” in *Proc. Fusion*, Jul. 2017, pp. 1–8.
- [36] G. Peyré and M. Cuturi, “Computational optimal transport: With applications to data science,” *Found. Trends Mach. Learn.*, vol. 11, no. 5–6, pp. 355–607, 2019.
- [37] N. Courty *et al.*, “Optimal transport for domain adaptation,” *IEEE Trans. Pattern Anal. Mach. Intell.*, vol. 39, no. 9, pp. 1853–1865, Sept. 2017.
- [38] C. Frogner *et al.*, “Learning with a wasserstein loss,” in *Proc. NIPS*, Dec. 2015, pp. 2053–2061.
- [39] O. Pele and M. Werman, “Fast and robust earth mover’s distances,” in *Proc. IEEE ICCV*, Sept. 2009, pp. 460–467.
- [40] S. Kolouri *et al.*, “Optimal mass transport: Signal processing and machine-learning applications,” *IEEE Signal Process. Mag.*, vol. 34, no. 4, pp. 43–59, Jul. 2017.
- [41] S. Taner *et al.*, “Channel charting in real-world coordinates with distributed MIMO,” *IEEE Trans. Wireless Commun.*, pp. 1–1, Apr. 2025.
- [42] B. Amos and J. Z. Kolter, “OptNet: Differentiable optimization as a layer in neural networks,” in *Proc. ICML*, Aug. 2017, pp. 136–145.
- [43] A. Agrawal *et al.*, “Differentiable convex optimization layers,” in *Proc. NeurIPS*, Dec. 2019.
- [44] H. Sun, Y. Shi, J. Wang, H. D. Tuan, H. V. Poor, and D. Tao, “Alternating differentiation for optimization layers,” in *Proc. ICLR*, May 2023.
- [45] M. Cuturi, “Sinkhorn distances: lightspeed computation of optimal transport,” in *Proc. NIPS*, Dec. 2013, pp. 2292–2300.
- [46] A. Genevay *et al.*, “Learning generative models with sinkhorn divergences,” in *Proc. AISTATS*, vol. 84, Apr. 2018, pp. 1608–1617.
- [47] J. B. Orlin, “A polynomial time primal network simplex algorithm for minimum cost flows,” *Mathematical Programming*, vol. 78, pp. 109–129, Aug. 1997.